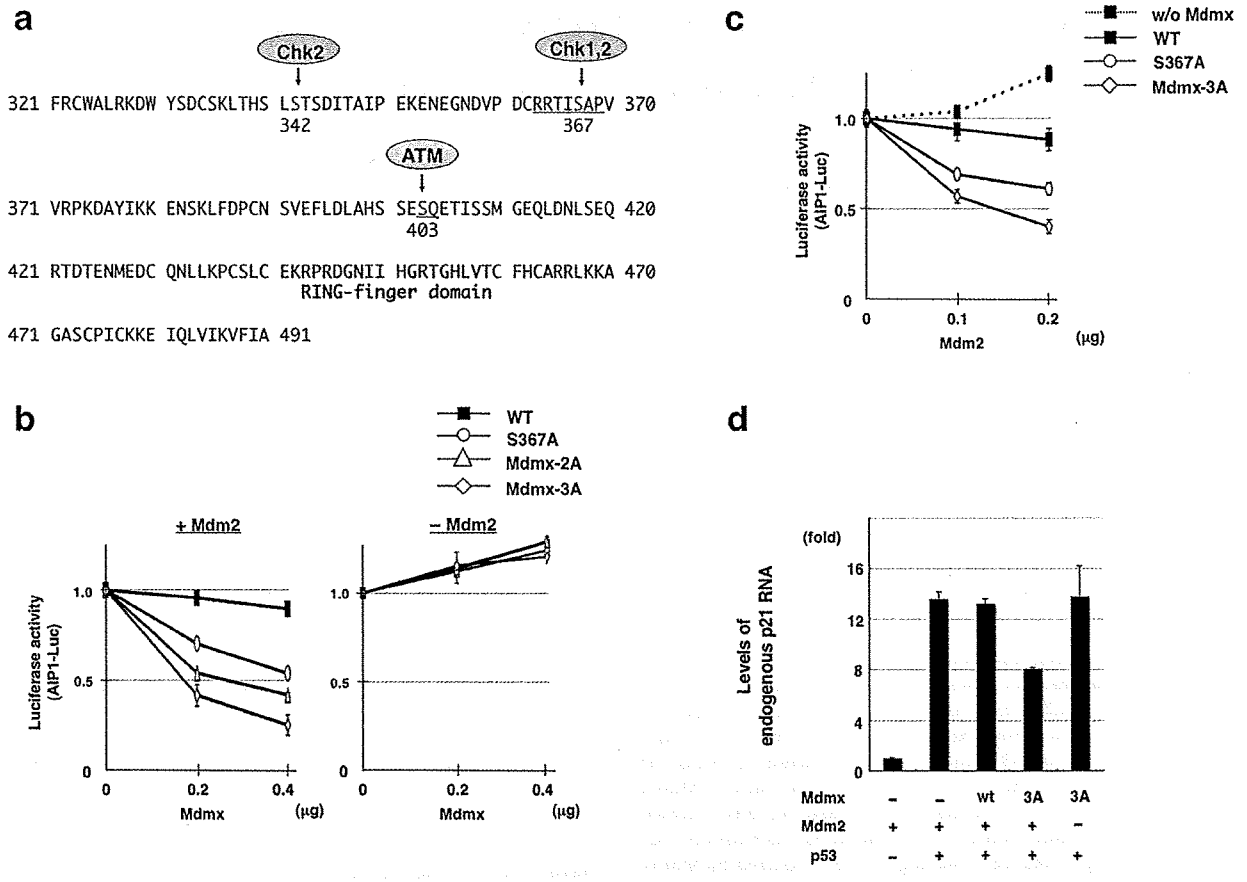

Fig. 1. Non-phosphorylatable Mdmx cooperates with Mdm2 to suppress p53. (a) Schematic representation of the positions of the Mdmx mutations. The serine residues phosphorylated after DNA damage are shown in red. The RING finger domain is shown in blue. (b,c) Inhibition of the transcriptional activity of p53 by the nonphosphorylatable mutants of Mdmx. (b) The indicated amounts of the wild-type Flag-Mdmx or Mdmx mutants were transfected into H1299 cells together with 0.15 μg HA-p53, 0.1 μg AIP-luc, and *Renilla* luciferase in the presence (left panel) or absence (right panel) of 0.2 μg myc-Mdm2. The total amount of transfected DNA was adjusted to 2 μg with pBluescript. Luciferase activity was measured 20 h after transfection. The numbers represent mean values ± standard deviations from experiments carried out in triplicate. The presented values were calculated as follows: value of cells transfected with the indicated amount of Mdmx/value of cells transfected without Mdmx. (c) The indicated amounts of myc-Mdm2 were transfected into H1299 cells together with 0.15 μg HA-p53, AIP-luc, *Renilla* luciferase, in the presence of 0.4 μg control vector, wild-type Flag-Mdmx, or the indicated Mdmx mutant. Luciferase assays were carried out as described in (b). (d) H1299 cells were cotransfected as described in (b). Total RNA prepared from transfected cells was used to measure the levels of endogenous p21 RNA by real-time RT-PCR using Taqman probe (Applied Biosciences, Foster City, CA). Levels of p21 were normalized with those of β-Actin.

shRNA infection. SH-SY5Y cells or IMR-32 cells were infected with lentiviruses as previously described.[21] Cells were infected with the control lentiviruses or the viruses that expressed the specific Mdmx shRNA overnight, incubated for an additional 2 days, and used for western blot analyses or immunostaining.

Additional information on Materials and Methods is provided in the Supporting Information.

Results

Non-phosphorylatable Mdmx effectively cooperates with Mdm2 to suppress p53 activity in H1299. Cellular stresses such as DNA damage cause degradation of Mdmx, via its phosphorylation by damage-induced kinases.[22] Serine 367 (S367) of Mdmx is phosphorylated after DNA damage, and alanine substitution of S367 (S367A), which mimics the nonphosphorylated form, promotes the cooperation between Mdmx and Mdm2 to inhibit p53 activity.[23] In addition to S367, two other serine residues comprise the major phosphorylation sites of Mdmx after DNA damage.[22] One of these sites, serine 403 (S403), is phosphorylated by ATM kinase,[22] whereas its downstream kinases, Chk1 or Chk2, phosphorylate serine 342 (S342) and S367, and facilitate the binding of 14-3-3 to Mdmx[22,24–26] (Fig. 1a). Phosphorylation of each site stimulates the proteasome-mediated degradation of Mdmx via its ubiquitination by Mdm2.[22,23,25]

Assuming that the phosphorylation of S342 and S403, in addition to S367, also compromises p53 suppression by Mdmx, we speculated that additional alanine substitution of S342 and S403 would allow Mdmx to inhibit p53 more effectively. We created the Mdmx mutants with the alanine substitution at S342 (Mdmx-2A) or at S342 plus S403 (Mdmx-3A) in addition to S367A, and introduced each mutant into p53-deficient H1299 cells together with p53 and the p53-responsive luciferase reporter (AIP-luc), in the presence or absence of the transfected Mdm2. Subsequently, the inhibitory effect of each Mdmx mutant on p53 activity was examined (Fig. 1b,c). Low amounts of Mdm2 were transfected so that introduction of Mdm2 alone did not inhibit p53 activity (Fig. 1c). As we reported previously,[23] the S367A mutation augmented the inhibition of p53 activity by Mdmx in the presence of transfected Mdm2 (Fig. 1b,c). The additional alanine substitution at S342 and S403 enhanced the ability of Mdmx to suppress p53 (Fig. 1b,c). In contrast, none of these mutants showed an inhibitory effect on p53 activity in the absence of the transfected Mdm2 (Fig. 1b). We observed similar Mdm2-dependent inhibition

doi: 10.1111/j.1349-7006.2009.01180.x

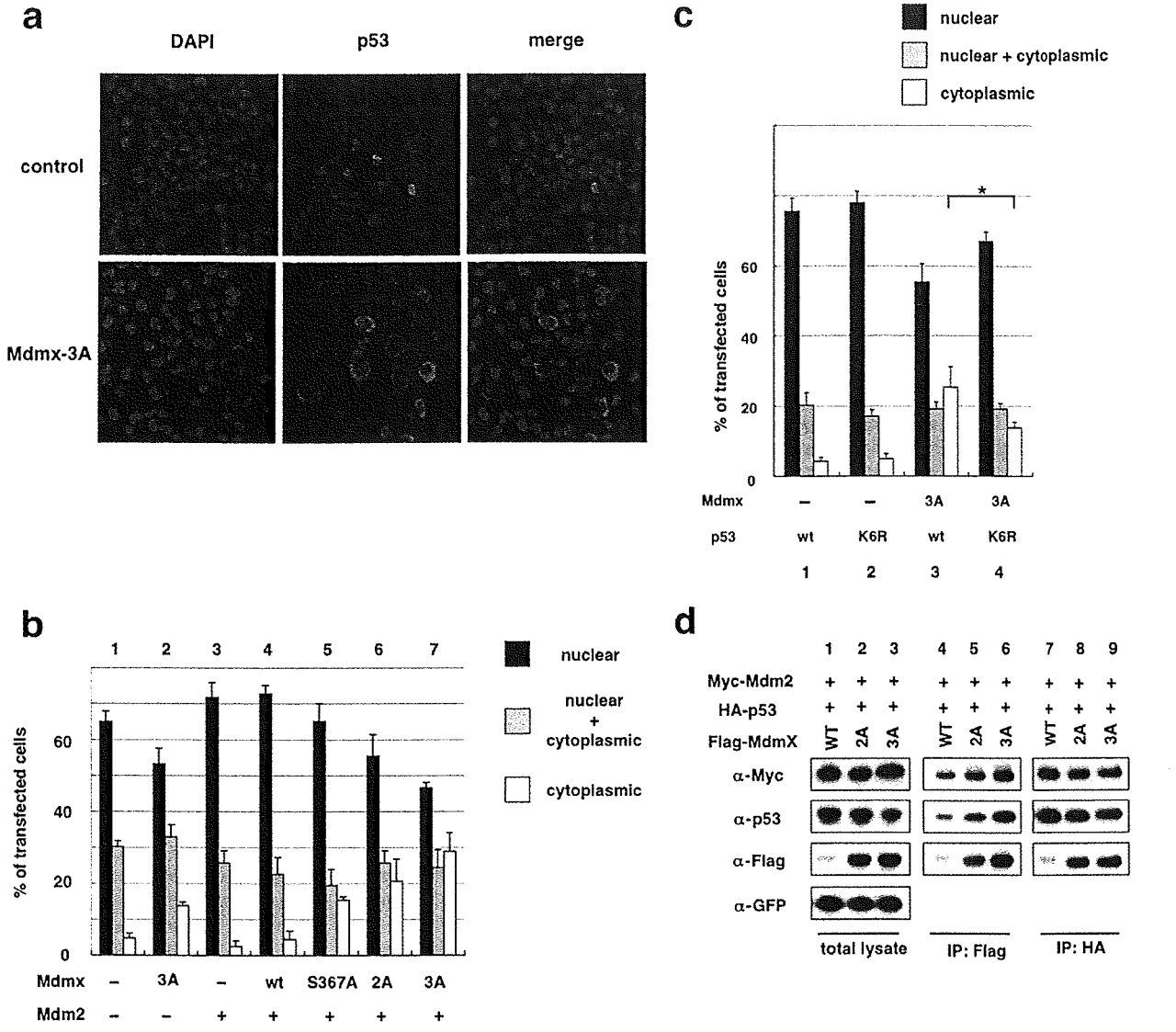

Fig. 2. Non-phosphorylatable Mdmx cooperates with Mdm2 to induce cytoplasmic localization of p53 in H1299. (a) H1299 cells were cotransfected with HA-p53 and myc-Mdm2, in the presence or absence of Mdmx-3A, and used for staining with DAPI and anti-HA antibody. Representative staining of the transfected cells is shown. (b) H1299 cells were cotransfected with the indicated Flag-Mdmx mutants and HA-p53 in the absence (columns 1 and 2) or presence (columns 3–7) of myc-Mdm2, and used for staining with anti-HA antibody. Subcellular localization of p53 of 100 transfected cells was evaluated in triplicate, and the average percentage of cells with the indicated staining pattern of p53 is shown. (c) Wild-type HA-p53 or HA-p53-K6R was transfected into H1299 cells together with myc-Mdm2 in the presence or absence of Flag-Mdmx-3A. Immunostaining analyses were carried out as described in (b). Asterisks indicate statistically significant differences ($P < 0.05$) as given by a one-way ANOVA followed by Tukey post-test. (d) HA-p53, myc-Mdm2, and GFP were transfected into H1299 together with the indicated Flag-tagged Mdmx as described in (b), and lysates prepared from transfected cells were used for immunoprecipitation (IP) with anti-Flag antibody (lanes 4–6) or anti-p53 (DO-1) antibody (lanes 7–9). The total lysates (lanes 1–3) and the immunoprecipitates were analysed by western blot analyses with the indicated antibodies.

of p53 activity by Mdmx-3A on another p53-responsive promoter (Bax-luc) (Supporting Information Fig. S1a). Wild-type Mdmx had an inhibitory effect that was comparable to that of Mdmx-3A in the presence of a chk2 inhibitor (Supporting Information Fig. S1b), suggesting that wild-type Mdmx is capable of inhibiting p53 in the absence of inhibitory phosphorylation.

Cotransfection of Mdm2 with these mutants suppressed the inhibitory effects of p53 on cell growth (Supporting Information Fig. S1c). In accordance with the inhibition of cell growth, Mdmx-3A, but not wild-type Mdmx, inhibits RNA expression of endogenous p21, which is a crucial target of p53 and inhibits cell cycle progression (Fig. 1d). Taken together, these data suggest that non-phosphorylated forms of Mdmx effectively cooperate with Mdm2 to inhibit p53 function.

Non-phosphorylatable Mdmx cooperates with Mdm2 to induce cytoplasmic localization of p53 in H1299. It has been demonstrated that low levels of Mdm2 inhibit p53 by inducing nuclear export.[27] In order to determine whether the nonphosphorylatable mutants of Mdmx cooperate with Mdm2 to inhibit p53 activity by stimulating cytoplasmic localization of p53, we next examined the subcellular localization of p53 after cotransfection of Mdmx, Mdm2, and p53 under the same conditions described in Figure 1(b). Introduction of Mdm2 alone did not significantly affect nuclear localization of p53 (Fig. 2a,b). Although cointroduction of Mdm2 and wild-type Mdmx had only a marginal effect on enhancement of cytoplasmic localization of p53 (Fig. 2b), cointroduction of Mdm2 and Mdmx-3A markedly enhanced a fraction of transfected cells with cytoplasmic p53 staining (Fig. 2a,b). Cytoplasmic

localization of p53 induced by Mdmx-3A alone was much less striking if compared to that induced by Mdm2 and Mdmx-3A (Fig. 2b), indicating that the effect of Mdmx-3A on the subcellular localization is largely dependent on the cointroduced Mdm2. Of note, there was a gradual enhancement of the cytoplasmic localization of p53 as Mdmx harbored an increasing number of alanine mutations at the phosphorylation sites (i.e. Mdmx-wt < S367A < 2A < 3A) (Fig. 2b), indicating that the extent of the stimulation of the cytoplasmic localization by the nonphosphorylatable mutations parallels their inhibitory effect on p53 activity (Fig. 1b). The cooperative effect of Mdmx-3A and Mdm2 to stimulate cytoplasmic localization of p53 was also observed in U2OS cells (Supporting Information Fig. S2a).

Cellular stresses such as DNA damage cause degradation of Mdmx via its phosphorylation by damage-induced kinases.[22,28] Mdmx was highly phosphorylated at S367 in transfected H1299[23] (K. Okamoto, unpublished data). In the presence of a chk2 inhibitor, wild-type Mdmx is capable of inducing cytoplasmic localization of p53 to an extent comparable to that of Mdmx-3A (Supporting Information Fig. S2b), indicating that in the absence of the inhibitory kinase, wild-type Mdmx is capable of inhibiting p53 activity (Supporting Information Fig. S1b) and inducing cytoplasmic localization of p53. These observations suggest that Mdmx phosphorylation may occur during the procedure of DNA transfection, and that the nonphosphorylatable Mdmx mutation facilitates clear observation of the cooperative effects of Mdmx and Mdm2 on p53 inhibition, by negating the inhibitory effects of Mdmx phosphorylation.

Mutation at the C-terminal lysines of p53 partially compromises the inhibitory effects of Mdmx-mediated enhancement of ubiquitination and inhibition of p53. It has been documented that Mdm2 ubiquitinates p53 at the six C-terminal lysines, the integrity of which are required for its nuclear export.[29,30] In addition to ubiquitination, some of these lysines are targeted for other types of modification, including neddylation, acetylation, and methylation.[31,32] Recent publications have indicated that Mdmx rescues the catalytic activity of Mdm2 mutants for ubiquitination and neddylation of p53 *in vivo*.[18,19,33] In order to determine whether Mdmx-3A enhances Mdm2-dependent p53 ubiquitination, we examined whether Mdmx enhances Mdm2-mediated ubiquitination in transfected H1299. Indeed, Mdmx-3A synergized with Mdm2 to induce p53 ubiquitination (Supporting Information Fig. S2c). In order to determine whether cooperative ubiquitination targets the C-terminal lysines of p53 by Mdmx and Mdm2, we created a mutant p53 in which all six lysines at the C-terminal domain were substituted with arginine (p53-K6R). *In vivo* ubiquitination assays confirmed that the K6R mutation eliminates the majority of p53 ubiquitination in transfected H1299 (data not shown). The K6R mutation partially inhibited Mdmx-3A-mediated cytoplasmic localization of p53 (Fig. 2c) and transcriptional inhibition of p53 (Supporting Information Fig. S2d). Thus, modification of the six lysines is partly required for Mdmx-dependent cytoplasmic localization and inactivation of p53, yet there exist other mechanisms by which Mdmx and Mdm2 cooperate to suppress p53 function.

Non-phosphorylatable mutations of Mdmx increase levels of the association of Mdmx to Mdm2 and p53. Next we determined whether the nonphosphorylatable mutations of Mdmx affect the levels of transfected p53, Mdm2, and Mdmx as well as the interaction among them (Fig. 2d). Mdmx-2A or Mdmx-3A expression did not markedly decrease the levels of p53 (Fig. 2d). In contrast, both the Mdmx-2A and Mdmx-3A mutations clearly increased the levels of introduced Mdmx (Fig. 2d). The levels of wild-type Mdmx and the Mdmx mutants were comparable in the presence of a proteasomal inhibitor MG132 (Supporting Information Fig. S2e), suggesting that the nonphosphorylatable mutations render Mdmx less sensitive to Mdm2-dependent proteasomal degradation.[22] In accordance with increased levels of Mdmx-2A and Mdmx-3A, the Mdmx mutations led to increased levels of the association of Mdmx to Mdm2 and p53 (Fig. 2d). These results indicate that the nonphosphorylatable mutations, by protecting Mdmx from Mdm2-dependent degradation, increase levels of the association of Mdmx to Mdm2 and p53.

Mdmx-3A mutation stimulates the association of Mdmx with Mdm2 and p53 predominantly in the cytoplasm. In order to examine whether the Mdmx-3A mutation affects subcellular localization of Mdmx and/or Mdm2 as well as p53, we next carried out immunostaining analyses of transfected Mdm2 and Mdmx. In agreement with a previous report,[10] transfected wild-type Mdmx was predominantly localized to the cytoplasm (Fig. 3a). Both wild-type Mdmx and Mdmx-3A mainly remained in the cytoplasm either in the presence or absence of cotransfected Mdm2 (Fig. 3a). Mdm2 predominantly localized to the nucleus in the absence of transfected Mdmx (Fig. 3b). Cotranfection of wild-type Mdmx mildly enhanced cytoplasmic localization of introduced Mdm2, and the extent of the cytoplasmic localization was markedly augmented by the Mdmx-3A mutation (Fig. 3b). Thus, the Mdmx-3A mutation facilitates cytoplasmic localization of cointroduced Mdm2.

The positive effects of Mdmx-3A mutation on the levels of the Mdmx–Mdm2 complex (Fig. 2d) and on the cytoplasmic localization of Mdm2 (Fig. 3b) suggest that the mutation leads to an increase of the Mdmx–Mdm2 complex in cytoplasm. Therefore, we next examined the extent of their interaction in each subcellular compartment after subcellular fractionation. In agreement with the results of the immunostaining (Fig. 3a,b), both Mdmx-3A and Mdm2 were mainly localized to the cytoplasm, and the Mdmx-3A–Mdm2 complex was predominantly formed in the cytoplasm (Fig. 3c). Cytoplasmic Mdmx-3A clearly colocalized with not only Mdm2 (data not shown) but also with p53 (Fig. 3d). Analyses of the subcellular localization of Mdmx-3A and p53 or of Mdmx-3A and Mdm2 in individual cells revealed that localization of Mdmx-3A in the cytoplasm was clearly associated with cytoplasmic localization of p53 (Supporting Information Fig. S3a) and Mdm2 (Supporting Information Fig. S3b). These data indicate that the Mdmx-3A mutation leads to an increase in the association of Mdmx with p53 and Mdm2 in the cytoplasm.

Cytoplasmic Mdmx is responsible for p53 localization in cytoplasm. In order to determine whether cytoplasmic Mdmx-3A induces localization of p53 to the cytoplasm, we generated Mdmx mutants in which either a peptide that corresponds to a nuclear localization signal of SV40 large T antigen (PKKKRKV) or a nuclear export signal of Rev of human immunodeficiency virus type-1 (LQLPPLERLTL) was connected to Mdmx-3A (NLS-Mdmx-3A or NES-Mdmx-3A). Subsequently, we introduced these Mdmx mutants together with Mdm2 and p53, and evaluated the effect of subcellular localization of Mdmx-3A on Mdm2 and p53. As expected, NLS-Mdmx-3A and NES-Mdmx-3A showed predominant localization to nuclei and cytoplasm respectively (Fig. 4a,b). Clear cytoplasmic localization of Mdm2 (Fig. 4c) and p53 (Fig. 4d) was induced by NES-Mdmx-3A, but not by NLS-Mdmx-3A. Inhibition of transcriptional activity of p53 by Mdmx-3A was enhanced by NES-Mdmx-3A and rather reduced by NLS-Mdmx-3A (Fig. 4e). Thus, cytoplasmic Mdmx-3A tethers p53 to the cytoplasm, whereas it effectively inhibits p53 activity in transfected H1299 cells.

Mdmx in the cytoplasm promotes cytoplasmic retention of endogenous p53. Next we examined whether subcellular localization of Mdmx-3A dictates localization of endogenous p53. Wild-type Mdmx, Mdmx-3A, NES-Mdmx-3A, or NLS-Mdmx-3A was introduced into U2OS cells, in which wild-type p53 is expressed predominantly in nuclei,[34] and we determined whether the mutants affect the subcellular localization of endogenous p53. The Mdmx-3A mutants were expressed at comparable levels (Fig. 4f). As we observed in H1299, NLS-Mdmx-3A and NES-Mdmx-3A predominantly localized to nuclei and cytoplasm respectively (data not shown). Introduction of wild-type Mdmx did not significantly affect nuclear localization of p53. In contrast, introduction of the

doi: 10.1111/j.1349-7006.2009.01180.x

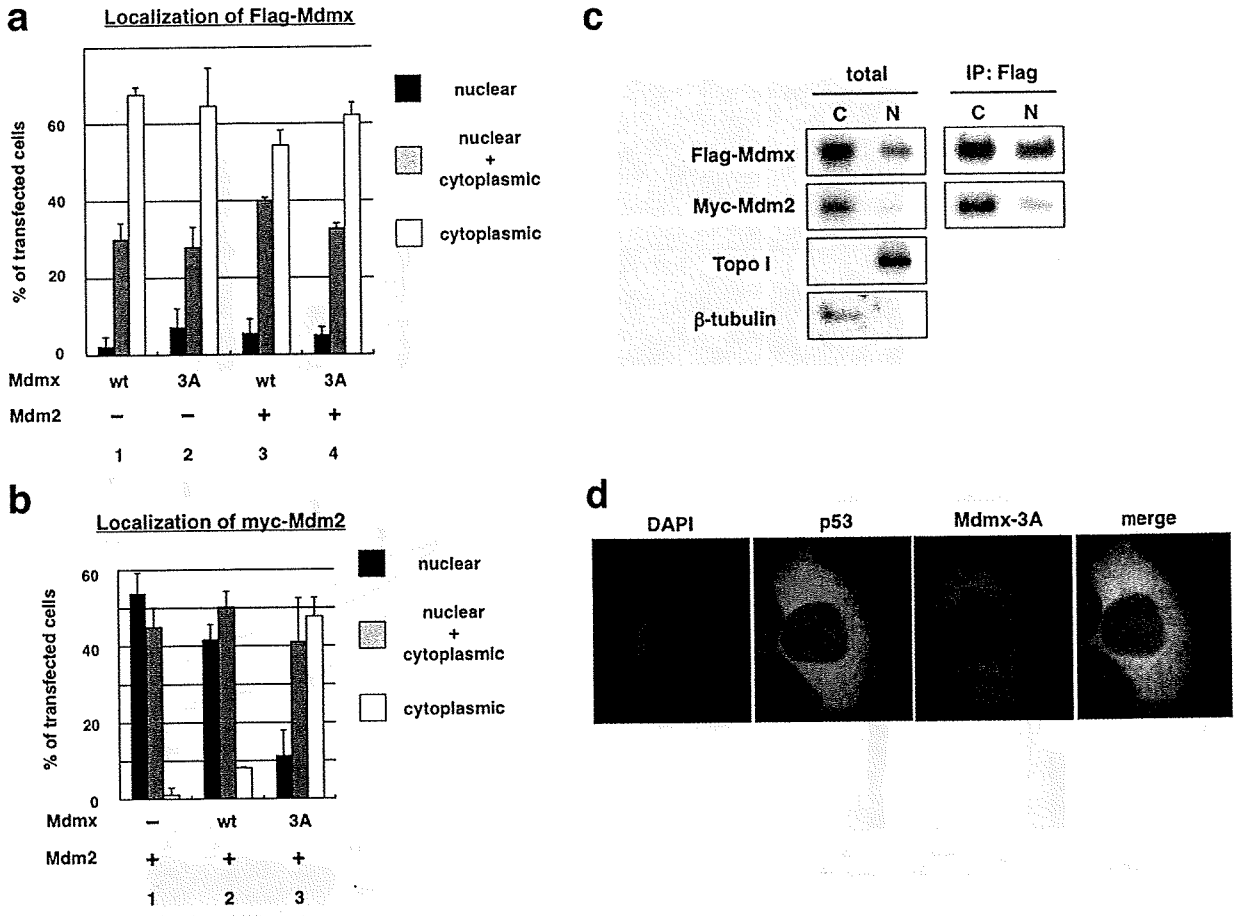

Fig. 3. The Mdmx-3A mutation stimulates the localization of Mdm2 and p53 predominantly to the cytoplasm. (a,b) HA-p53 was transfected into H1299 cells together with the indicated Flag-Mdmx in the presence or absence of myc-Mdm2 as described in Figure 2(b). The transfected cells were sequentially immunostained with (a) anti-Flag (M2) antibody or (b) antimyc antibody, antimouse IgG antibody conjugated with Alexa 595, and anti-HA antibody conjugated with Alexa 488 (Molecular Probe). Subcellular localization of (a) Flag-Mdmx or (b) myc-Mdm2 in cells that express HA-p53 was evaluated as described in Figure 2(b). (c) H1299 cells were transfected with HA-p53 together with Flag-Mdmx-3A and myc-Mdm2. The transfected cells were subjected to subcellular fractionation. The total lysates and the Flag-immunoprecipitates were then used for western blot analyses with the indicated antibodies. Topoisomerase I and γ tubulin are shown as nuclear and cytoplasmic markers respectively. (d) Representative staining of cells that express cytoplasmic p53 and Mdmx.

Mdmx-3A mutants induced localization of p53 to the cytoplasm, and a striking enhancement of cytoplasmic localization of p53 was observed in the presence of NES-Mdmx-3A (Fig. 4f). Taken together, these data indicate that cytoplasmically located Mdmx, presumably by tethering p53, induces localization of endogenous p53 to the cytoplasm.

Both Mdmx and Mdm2 predominantly localize to the cytoplasm of neuroblastoma cells. Inactivation of p53 via its cytoplasmic localization is frequently observed in some types of cancer such as neuroblastoma,[35] and yet the precise mechanism by which p53 is sequestered in cytoplasm remains obscure. It was reported that Mdm2 mediates the cytoplasmic retention of p53 in neuroblastoma.[36,37] In order to examine whether Mdmx as well as Mdm2 is involved in p53 inactivation via cytoplasmic sequestration in neuroblastoma, we analyzed SH-SY5Y and IMR-32 cells that, like most other neuroblastoma cells, harbor wild-type p53 with cytoplasmic localization (Fig. 5a; Supporting Information Fig. S4a). Expression levels of Mdmx in SH-SY5Y were much higher than those in normal human fibroblasts, and even higher than those in MCF-7 (data not shown), breast cancer cells in which the *mdmx* gene is amplified and Mdmx is expressed at high levels.[38] Both Mdmx and Mdm2 predominantly localized to the cytoplasm in SH-SY5Y cells (Supporting Information Fig. S4a). The extent of S367 phosphorylation in SH-5YSY cells was much lower than that in the transfected H1299 cells (Supporting Information Fig. S4c). These observations suggest that Mdmx is expressed, probably in nonphosphorylated forms, at high levels in the cytoplasm in unstressed SH-SY5Y cells.

Nuclear Mdmx inhibits cytoplasmic retention of p53 in SH-5Y5Y. In order to determine whether subcellular localization of Mdmx-3A dictates localization of endogenous p53 in neuroblastoma cells as well as in U2OS cells, the effects of subcellular localization of wild-type Mdmx or the Mdmx mutants on endogenous p53 localization were evaluated as described in Figure 4(f). The Mdmx-3A mutants were expressed at comparable levels (Fig. 5b). In accordance with cytoplasmic localization of endogenous Mdmx (Supporting Information Fig. S4a), Mdmx-3A and wild-type Mdmx exclusively localized to the cytoplasm (Fig. 5b). As expected, the majority of NLS-Mdmx-3A localized to nuclei (87%) and NES-Mdmx-3A totally localized to the cytoplasm. Immunostaining of transfected SH-SY5Y cells revealed that the expression of NLS-Mdmx-3A, but not NES-Mdmx-3A, reduced cytoplasmic localization of p53 (Fig. 5b), indicating that nuclear expression of Mdmx-3A inhibits cytoplasmic retention of p53 in SH-SY5Y.

Mdmx is required for inactivation of p53 in neuroblastoma cells. In order to further examine the role of Mdmx in p53 inactivation

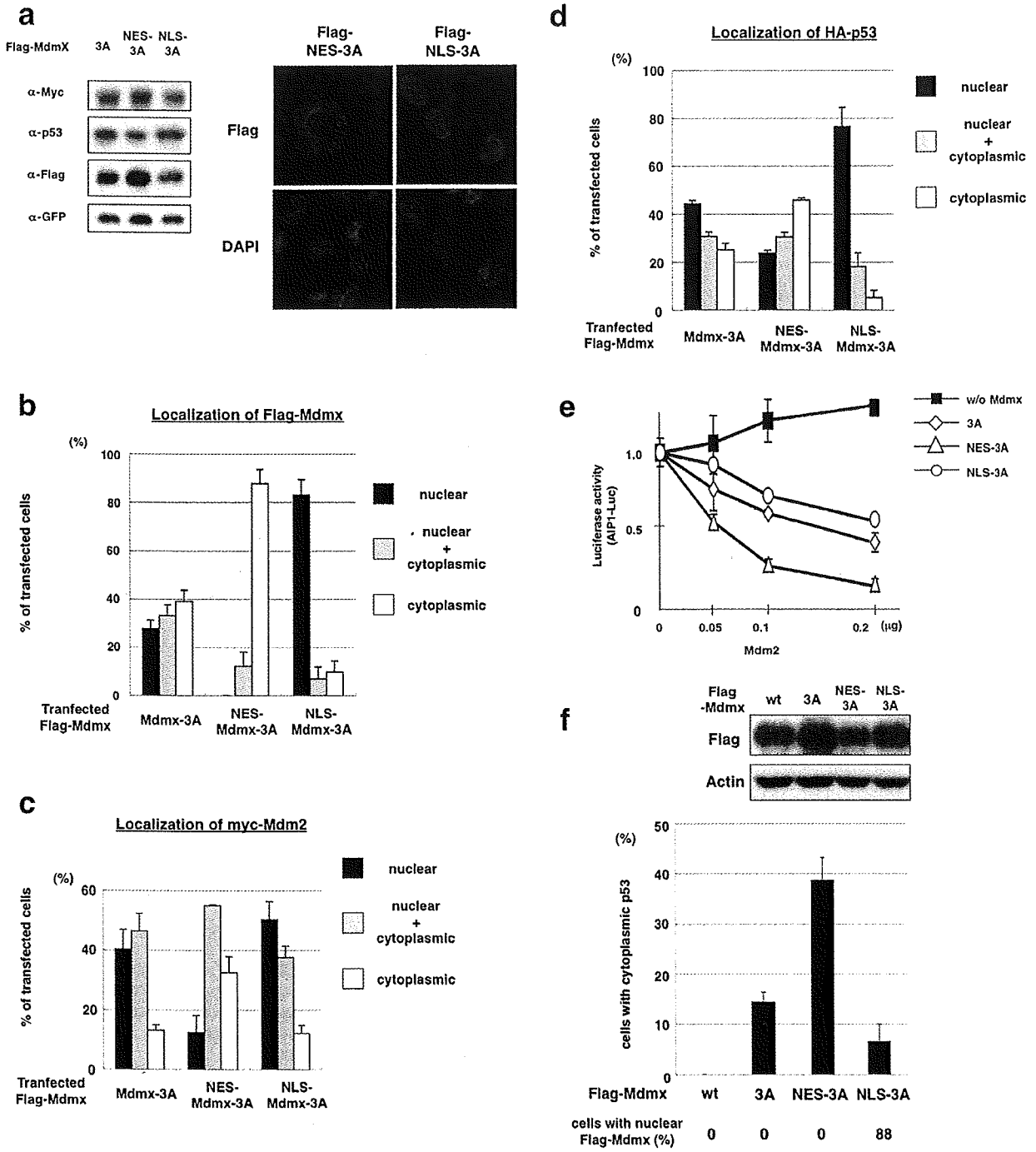

Fig. 4. Cytoplasmic Mdmx tethers p53 and Mdm2 to the cytoplasm and stimulates p53 inhibition. (a) H1299 cells were cotransfected with HA-p53, myc-Mdm2, GFP, and the indicated Flag-tagged Mdmx. Left panel, western blot analyses with the indicated antibodies. Right panel, representative staining with anti-Flag antibody and DAPI. (b–d) H1299 cells were transfected with the indicated Mdmx, together with myc-Mdm2, and immunostained with (b) anti-Flag antibody, (c) anti-Mdm2 antibody, or (d) anti-HA antibody. Subcellular localization of transfected (b) Mdmx, (c) Mdm2, or (d) p53 was represented as described in Figure 2(b). (e) Flag-Mdmx mutant or the control vector was transfected into H1299 cells together with HA-p53, in the presence of the indicated amounts of myc-Mdm2, and luciferase assays were carried out as described in Figure 1(c). (f) U2OS cells were transfected with the indicated Flag-Mdmx. Upper panel, western blot analyses with the anti-Flag or the anti-actin antibodies. Lower panel, cells transfected with the indicated plasmids were immunostained with the anti-Flag and antip53 (CM1) antibodies, and a fraction of the transfected cells with cytoplasmic p53 staining was quantified.

in neuroblastoma cells, we inhibited Mdmx expression by infecting cells with the lentiviruses expressing Mdmx shRNA. Mdmx inhibition by the specific shRNA, while not significantly affecting levels of p53, induced expression of p21, a crucial p53 target (Fig. 5c) and reduced the cytoplasmic localization of p53 (Fig. 5d,e). The positive role of Mdmx in cytoplasmic localization of p53 was confirmed by western blot analyses of nuclear and cytoplasmic lysates prepared from the infected cells. Depletion of Mdmx

doi: 10.1111/j.1349-7006.2009.01180.x

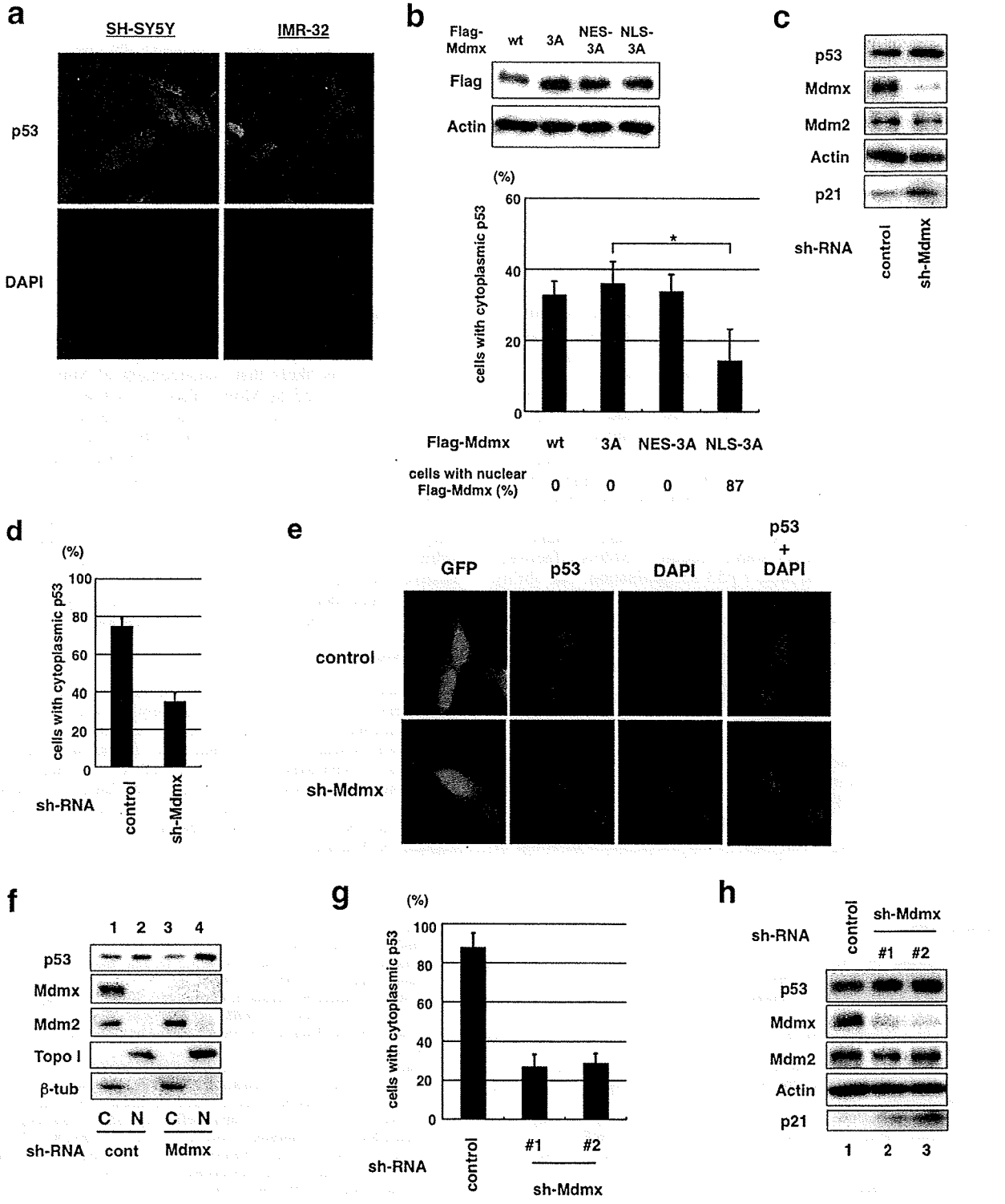

Fig. 5. Mdmx is required for cytoplasmic retention of p53 in neuroblastoma cells. (a) Cytoplasmic retention of p53 in neuroblastoma. SH-SY5Y or IMR-32 cells were stained with antip53 antibody (CM1) and DAPI. (b) SH-SY5Y cells were transfected with the indicated Flag-tagged Mdmx. Western blot analyses and quantification of a fraction of cells with cytoplasmic p53 were carried out as described in Figure 4(f). (c–f) SH-SY5Y cells were infected with the control lentivirus or the viruses expressing Mdmx shRNA. (c) Lysates prepared from the infected cells were used for western blot analyses with the indicated antibodies. (d) The infected cells were immunostained with antip53 polyclonal antibody (CM1) and DAPI. The average percentage of the infected cells with cytoplasmic staining of p53 was presented after evaluating subcellular localization of p53 of 100 cells in triplicate. (e) Representative pictures of staining of cells that were infected with the control lentiviruses or the viruses that express Mdmx shRNA. Note that the viruses express GFP, and infection efficiency is ~100% judging from GFP expression. (f) Subcellular fractionation and western blot analyses were carried out with the indicated antibodies. (g,h) IMR-32 cells were infected with the control lentiviruses or the viruses that express Mdmx shRNA, and (g) western blot analyses or (h) the quantification of subcellular distribution of p53 was carried out as described in (c) and (d) respectively.

decreased p53 levels in the cytoplasm and increased those in nuclei, while the depletion did not significantly affect cytoplasmic localization of Mdm2 (Fig. 5f).

Similarly, inhibition of Mdmx by the specific shRNA led to induction of p21 expression and inhibition of cytoplasmic localization of p53 in IMR-32, another neuroblastoma cell line (Fig. 5g,h; Supporting Information Fig. S4c). Thus, Mdmx contributes to cytoplasmic retention of p53 in neuroblastoma cells.

Discussion

Genetic evidence indicates that *mdmx* is a crucial inhibitor of p53 and that *mdmx* and *mdm2* cooperatively function to inhibit p53. However, the mechanical basis of the cooperation of the oncogenes is not clearly established. In an attempt to recapitulate synergistic inhibition of p53 by Mdmx and Mdm2, we took advantage of our observation that the nonphosphorylatable mutations confer Mdmx resistance against Mdm2-mediated degradation. We demonstrated that nonphosphorylatable mutations of Mdmx markedly enhance the ability of Mdmx to cooperate with Mdm2 for inhibition of p53, suggesting that the stress-induced phosphorylation of Mdmx is important for its ability to suppress p53. The importance of the Mdmx phosphorylation was further supported by the functionality of wild-type Mdmx on p53 suppression in the presence of a chk2 inhibitor (Supporting Information Figs S1b and 2b).

Through the analyses of the function of the Mdmx mutants, we found that the nonphosphorylatable mutant of Mdmx effectively cooperates with Mdm2 to induce p53 ubiquitination. The ability of the nonphosphorylatable mutations of Mdmx to inhibit p53 activity was associated with enhanced cytoplasmic retention of p53 and with increased levels of the interaction of Mdmx to p53 and Mdm2 in cytoplasm. A causal role of cytoplasmic Mdmx to induce localization of p53 in the cytoplasm was demonstrated using the Mdmx mutants that harbor autonomous subcellular localization signals.

p53 is sequestered in the cytoplasm in some types of cancer, and it is assumed that the sequestration of p53 contributes to p53 inactivation.[35,39] Mdm2 is essential for inhibition and cytoplasmic sequestration of p53 in neuroblastoma cells,[36,37] and the cooperative function of Mdmx and Mdm2 to induce p53 retention in the cytoplasm may contribute to its inactivation in some of cancer cells. We found that, in addition to Mdm2, Mdmx is also required for cytoplasmic sequestration of p53 in neuroblastoma cells. Considering that Mdm2 enhances the interaction between p53 and Mdmx in the transfected H1299 cells, Mdmx and Mdm2 may cooperate by stimulating the formation of a complex with p53. Of note, Mdmx stabilizes p53 via a formation of a complex with Mdm2,[16] and formation of such a stable complex may account for cytoplasmic sequestration of p53.

In addition to the cytoplasmic tethering via physical interaction, regulation of post-translational modification of the C-terminal of p53 is likely to contribute to the cooperative inhibition of p53 by Mdm2 and Mdmx, because mutations in the six C-terminal lysines, which are targets for the regulatory modification, partly abolished the cooperative inhibition of p53 (Supporting Information Fig. S2d). Mdm2 promotes cytoplasmic translocation of p53 via its ubiquitination at the same lysine residues,[27,40] and accumulating data[9,18,19] as well as ours (Supporting Information Fig. 2c) indicate that Mdmx promotes Mdm2-dependent p53 ubiquitination. Hence, it is likely that enhancement of Mdm2-dependent ubiquitination of p53 by Mdmx also contributes to the cooperative inhibition of p53 activity by these oncoproteins. In fact, the cytoplasmic retention of p53 in neuroblastoma is in part attributed to multimono-ubiquitination of p53 due to defective function of HAUSP, a de-ubiquitinating enzyme for p53 and Mdmx and Mdm2.[34,41,42] However, we did not observe a significant change in the pattern of p53 laddering, which presumably represents ubiquitinated p53, in neuroblastoma cells after knock down of Mdmx (data not shown). The two mechanisms that mediate cytoplasmic localization of p53, namely cytoplasmic tethering and ubiquitin-dependent translocation, are not mutually exclusive, and presumably contribute to cytoplasmic retention of p53 by Mdmx.

Acknowledgments

We are indebted to Jiandong Chen and Hirofumi Arakawa for providing us with Flag-Mdm2 and AIP-luc respectively. We thank Kenji Kashima for experimental assistance. This work was supported by a Grant-in-Aid for Scientific Research from the Ministry of Education, Culture, Sports, Science, and Technology of Japan (Y.T. and K.O.), a Grant-in-Aid for Third Term Comprehensive Control Research for Cancer from the Ministry of Health, Labor, and Welfare, Japan (Y.T.), the Foundation for Promotion of Cancer Research (K.O.), and the Japan–France Integrated Action Program (K.O. and C.G.).

References

1 Braithwaite AW, Prives CL. p53: more research and more questions. *Cell Death Differ* 2006; **13**: 877–80.
2 Levine AJ. p53, the cellular gatekeeper for growth and division. *Cell* 1997; **88**: 323–31.
3 Oren M. Decision making by p53: life, death and cancer. *Cell Death Differ* 2003; **10**: 431–42.
4 Ko LJ, Prives C. p53: puzzle and paradigm. *Genes Dev* 1996; **10**: 1054–72.
5 Vogelstein B, Lane D, Levine AJ. Surfing the p53 network. *Nature* 2000; **408**: 307–10.
6 Toledo F, Wahl GM. MDM2 and MDM4: p53 regulators as targets in anticancer therapy. *Int J Biochem Cell Biol* 2007; **39**: 1476–8.
7 Marine JC, Dyer MA, Jochemsen AG. MDMX: from bench to bedside. *J Cell Sci* 2007; **120**: 371–8.
8 Marine JC, Francoz S, Maetens M, Wahl G, Toledo F, Lozano G. Keeping p53 in check: essential and synergistic functions of Mdm2 and Mdm4. *Cell Death Differ* 2006; **13**: 927–34.
9 Linares LK, Hengstermann A, Ciechanover A, Muller S, Scheffner M. HdmX stimulates Hdm2-mediated ubiquitination and degradation of p53. *Proc Natl Acad Sci USA* 2003; **100**: 12 009–14.
10 Gu J, Kawai H, Nie L *et al.* Mutual dependence of MDM2 and MDMX in their functional inactivation of p53. *J Biol Chem* 2002; **277**: 19 251–4.
11 Tanimura S, Ohtsuka S, Mitsui K, Shirouzu K, Yoshimura A, Ohtsubo M. MDM2 interacts with MDMX through their RING finger domains. *FEBS Lett* 1999; **447**: 5–9.
12 Sharp DA, Kratowicz SA, Sank MJ, George DL. Stabilization of the MDM2 oncoprotein by interaction with the structurally related MDMX protein. *J Biol Chem* 1999; **274**: 38 189–96.
13 Michael D, Oren M. The p53–Mdm2 module and the ubiquitin system. *Semin Cancer Biol* 2003; **13**: 49–58.
14 Honda R, Tanaka H, Yasuda H. Oncoprotein MDM2 is a ubiquitin ligase E3 for tumor suppressor p53. *FEBS Lett* 1997; **420**: 25–7.
15 Coutts AS, La Thangue NB. Mdm2 widens its repertoire. *Cell Cycle* 2007; **6**: 827–9.
16 Stad R, Little NA, Xirodimas DP *et al.* Mdmx stabilizes p53 and Mdm2 via two distinct mechanisms. *EMBO Rep* 2001; **2**: 1029–34.
17 Toledo F, Krummel KA, Lee CJ *et al.* A mouse p53 mutant lacking the proline-rich domain rescues Mdm4 deficiency and provides insight into the Mdm2-Mdm4-p53 regulatory network. *Cancer Cell* 2006; **9**: 273–85.
18 Poyurovsky MV, Priest C, Kentsis A *et al.* The Mdm2 RING domain C-terminus is required for supramolecular assembly and ubiquitin ligase activity. *EMBO J* 2007; **26**: 90–101.
19 Uldrijan S, Pannekoek WJ, Vousden KH. An essential function of the extreme C-terminus of MDM2 can be provided by MDMX. *EMBO J* 2007; **26**: 102–12.
20 Shinozaki T, Nota A, Taya Y, Okamoto K. Functional role of Mdm2 phosphorylation by ATR in attenuation of p53 nuclear export. *Oncogene* 2003; **22**: 8870–80.
21 Laurie NA, Donovan SL, Shih CS *et al.* Inactivation of the p53 pathway in retinoblastoma. *Nature* 2006; **444**: 61–6.
22 Pereg Y, Shkedy D, de Graaf P *et al.* Phosphorylation of Hdmx mediates its Hdm2- and ATM-dependent degradation in response to DNA damage. *Proc Natl Acad Sci USA* 2005; **102**: 5056–61.

doi: 10.1111/j.1349-7006.2009.01180.x

23 Okamoto K, Kashima K, Pereg Y *et al.* DNA damage-induced phosphorylation of MdmX at serine 367 activates p53 by targeting MdmX for Mdm2-dependent degradation. *Mol Cell Biol* 2005; **25**: 9608–20.
24 Jin Y, Dai MS, Lu SZ *et al.* 14-3-3gamma binds to MDMX that is phosphorylated by UV-activated Chk1, resulting in p53 activation. *EMBO J* 2006; **25**: 1207–18.
25 Pereg Y, Lam S, Teunisse A *et al.* Differential roles of ATM- and Chk2-mediated phosphorylations of Hdmx in response to DNA damage. *Mol Cell Biol* 2006; **26**: 6819–31.
26 Chen L, Gilkes DM, Pan Y, Lane WS, Chen J. ATM and Chk2-dependent phosphorylation of MDMX contribute to p53 activation after DNA damage. *EMBO J* 2005; **24**: 3411–22.
27 Shmueli A, Oren M. Regulation of p53 by Mdm2: fate is in the numbers. *Mol Cell* 2004; **13**: 4–5.
28 Lopez-Pajares V, Kim MM, Yuan ZM. Phosphorylation of MDMX mediated by Akt leads to stabilization and induces 14-3-3 binding. *J Biol Chem* 2008; **283**: 13707–13.
29 Gu J, Nie L, Wiederschain D, Yuan ZM. Identification of p53 sequence elements that are required for MDM2-mediated nuclear export. *Mol Cell Biol* 2001; **21**: 8533–46.
30 Lohrum MA, Woods DB, Ludwig RL, Balint E, Vousden KH. C-terminal ubiquitination of p53 contributes to nuclear export. *Mol Cell Biol* 2001; **21**: 8521–32.
31 Xirodimas DP, Saville MK, Bourdon JC, Hay RT, Lane DP. Mdm2-mediated NEDD8 conjugation of p53 inhibits its transcriptional activity. *Cell* 2004; **118**: 83–97.
32 Toledo F, Wahl GM. Regulating the p53 pathway: *in vitro* hypotheses, *in vivo* veritas. *Nat Rev Cancer* 2006; **6**: 909–23.
33 Singh RK, Iyappan S, Scheffner M. Hetero-oligomerization with MdmX rescues the ubiquitin/Nedd8 ligase activity of RING finger mutants of Mdm2. *J Biol Chem* 2007; **282**: 10 901–7.
34 Becker K, Marchenko ND, Maurice M, Moll UM. Hyperubiquitylation of wild-type p53 contributes to cytoplasmic sequestration in neuroblastoma. *Cell Death Differ* 2007; **14**: 1350–60.
35 Moll UM, LaQuaglia M, Benard J, Riou G. Wild-type p53 protein undergoes cytoplasmic sequestration in undifferentiated neuroblastomas but not in differentiated tumors. *Proc Natl Acad Sci USA* 1995; **92**: 4407–11.
36 Lu W, Pochampally R, Chen L, Traidej M, Wang Y, Chen J. Nuclear exclusion of p53 in a subset of tumors requires MDM2 function. *Oncogene* 2000; **19**: 232–40.
37 Rodriguez-Lopez AM, Xenaki D, Eden TO, Hickman JA, Chresta CM. MDM2 mediated nuclear exclusion of p53 attenuates etoposide-induced apoptosis in neuroblastoma cells. *Mol Pharmacol* 2001; **59**: 135–43.
38 Danovi D, Meulmeester E, Pasini D *et al.* Amplification of Mdmx (or Mdm4) directly contributes to tumor formation by inhibiting p53 tumor suppressor activity. *Mol Cell Biol* 2004; **24**: 5835–43.
39 Jimenez GS, Khan SH, Stommel JM, Wahl GM. p53 regulation by post-translational modification and nuclear retention in response to diverse stresses. *Oncogene* 1999; **18**: 7656–65.
40 Li M, Brooks CL, Wu-Baer F, Chen D, Baer R, Gu W. Mono-versus polyubiquitination: differential control of p53 fate by Mdm2. *Science* 2003; **302**: 1972–5.
41 Li M, Brooks CL, Kon N, Gu W. A dynamic role of HAUSP in the p53–Mdm2 pathway. *Mol Cell* 2004; **13**: 879–86.
42 Meulmeester E, Maurice MM, Boutell C *et al.* Loss of HAUSP-mediated deubiquitination contributes to DNA damage-induced destabilization of Hdmx and Hdm2. *Mol Cell* 2005; **18**: 565–76.

Supporting Information

Additional Supporting Information may be found in the online version of this article:

Supporting Information Materials and Methods

Fig. S1. Non-phosphorylatable Mdmx cooperates with Mdm2 to suppress p53.

Fig. S2. Non-phosphorylatable Mdmx cooperates with Mdm2 to induce cytoplasmic localization of p53 in H1299.

Fig. S3. The Mdmx-3A mutation stimulates the localization of Mdm2 and p53 predominantly to the cytoplasm.

Fig. S4. Mdmx is required for cytoplasmic retention of p53 in neuroblastoma cells.

Please note: Wiley-Blackwell are not responsible for the content or functionality of any supporting materials supplied by the authors. Any queries (other than missing material) should be directed to the corresponding author for the article.

Stress-Activated Mitogen-Activated Protein Kinases c-Jun NH_2-Terminal Kinase and p38 Target Cdc25B for Degradation

Sanae Uchida,[1,2] Katsuji Yoshioka,[3] Ryoichi Kizu,[4] Hitoshi Nakagama,[5] Tsukasa Matsunaga,[1] Yukihito Ishizaka,[6] Randy Y.C. Poon,[7] and Katsumi Yamashita[1]

[1]Division of Life Science, Graduate School of Natural Science and Technology, [2]Venture Business Laboratory, Center for Innovation, and [3]Division of Molecular Cell Signaling, Cancer Research Institute, Kanazawa University, Kanazawa, Japan; [4]Laboratory of Environmental Biochemistry, Faculty of Pharmaceutical Science, Doshisha Women's College of Liberal Arts, Kyotanabe, Japan; [5]Division of Biochemistry, National Cancer Center Research Institute; [6]Division of Intractable Diseases, Research Institute, International Medical Center of Japan, Tokyo, Japan; and [7]Department of Biochemistry, Hong Kong University of Science and Technology, Clear Water Bay, Hong Kong

Abstract

Cdc25 dual specificity phosphatases positively regulate the cell cycle by activating cyclin-dependent kinase/cyclin complexes. Of the three mammalian Cdc25 isoforms, Cdc25A is phosphorylated by genotoxic stress–activated Chk1 or Chk2, which triggers its $SCF^{\beta\text{-}TrCP}$–mediated degradation. However, the roles of Cdc25B and Cdc25C in cell stress checkpoints remain inconclusive. We herein report that c-Jun NH_2-terminal kinase (JNK) induces the degradation of Cdc25B. Nongenotoxic stress induced by anisomycin caused rapid degradation of Cdc25B as well as Cdc25A. Cdc25B degradation was dependent mainly on JNK and partially on p38 mitogen-activated protein kinase (p38). Accordingly, cotransfection with JNK1, JNK2, or p38 destabilized Cdc25B. *In vitro* kinase assays and site-directed mutagenesis experiments revealed that the critical JNK and p38 phosphorylation site in Cdc25B was Ser^{101}. Cdc25B with Ser^{101} mutated to alanine was refractory to anisomycin-induced degradation, and cells expressing such mutant Cdc25B proteins were able to override the anisomycin-induced G_2 arrest. These results highlight the importance of a novel JNK/p38-Cdc25B axis for a nongenotoxic stress–induced cell cycle checkpoint. [Cancer Res 2009;69(16):6438–44]

Introduction

Cell cycle progression in eukaryotic cells requires the successive activation and inactivation of cyclin-dependent kinase (CDK)-cyclin complexes. Activation of CDK-cyclin complexes depends on members of the Cdc25 dual specificity phosphatases. In mammalian cells, the Cdc25 family consists of Cdc25A, Cdc25B, and Cdc25C. Although Cdc25C was the first member to be identified, Cdc25A is now regarded as one of the major players in multiple phases of cell cycle progression in mammalian somatic cells (1, 2). Besides its well-known role in G_1-S transition, Cdc25A is also involved in the G_2-M transition and chromosome condensation (1, 3, 4). Moreover, Cdc25A is also a well-known target of the DNA damage checkpoint (2, 5). On genotoxic insults, Cdc25A is rapidly phosphorylated by the checkpoint kinases Chk1 and Chk2 followed by $SCF^{\beta\text{-}TrCP}$–mediated ubiquitinylation and degradation (2, 6).

In contrast to Cdc25A, the roles of Cdc25B and Cdc25C remain elusive. Experiments with Cdc25B- or Cdc25C-knockout mice indicate that these genes are dispensable not only for normal cell cycle control but also for the DNA damage checkpoint (7, 8). The only prominent phenotype is a defect in oocyte maturation in Cdc25B-depleted female mice (9). However, several lines of evidence suggest that Cdc25B is important for controlling CDK1-cyclin B activity at the centrosome, where the kinase contributes to centrosome separation at prophase (4, 10). Chk1 is believed to down-regulate the activity of Cdc25B until prophase (11, 12). The phosphorylation of Cdc25B (Ser^{309} of Cdc25B1 or Ser^{323} in Cdc25B3) has also been implicated in the function of Cdc25B in conjunction with 14-3-3 binding (13, 14). A mutation that abolishes the specific phosphorylation site causes Cdc25B to localize to the nucleus and enhances its ability to abrogate DNA damage–induced G_2 arrest (15, 16). These results suggest that despite its nonessentiality in mouse models, Cdc25B does play some role in the G_2-M transition (14).

Stress stimuli that do not target genome DNA lead to the activation of the so-called stress-activated mitogen-activated protein kinases (MAPK), including p38 MAPK (p38) and c-Jun NH_2-terminal kinase (JNK; ref. 17). Recently, MAPKAP kinase 2 (MK2) has received attention for its ability to phosphorylate Cdc25B, leading to 14-3-3 binding (18). MK2 is usually complexed with and activated by p38 (18). Therefore, a fraction of p38 can be found to coimmunoprecipitate with MK2, which could mislead one to believe that p38 phosphorylates substrates that are normally phosphorylated exclusively by MK2. The p38-MK2 cascade is, therefore, believed to regulate cell cycle progression by controlling the stability and subcellular localization of Cdc25A and Cdc25B, respectively, when cells are exposed to genotoxic or nongenotoxic stress (14, 18–20). JNK also phosphorylates and inactivates Cdc25C (21). In addition, nuclear Cdc25B is exported to the cytoplasm on UV or nongenotoxic stress by an unknown mechanism (22).

We previously reported that overexpression of 14-3-3 causes the relocation of Cdc25B from the nucleus to the cytoplasm (13, 23, 24). To delineate the role of the cytoplasmic export of Cdc25B, we established HeLa cell lines that constitutively express Cdc25B and investigated conditions that induce nuclear export of the phosphatase. We found that nongenotoxic stress, but not genotoxic cell stress, induced loss of Cdc25B nuclear localization and that nongenotoxic stress was also an effective inducer of Cdc25B degradation. Moreover, we found that the stability of Cdc25B could be controlled by JNK and p38. These data reveal a novel pathway linking the stress response kinases to the G_2-M cell cycle engine.

Materials and Methods

Reagents, plasmids, and antibodies. Reagents of the highest grade were obtained from Wako or Sigma. Restriction enzymes were obtained from New England Biolabs, and MKK7-activated recombinant JNK1 and

Note: Supplementary data for this article are available at Cancer Research Online (http://cancerres.aacrjournals.org/).

Requests for reprints: Katsumi Yamashita, Division of Life Sciences, Graduate School of Natural Science and Technology, Kanazawa University, Kakuma-machi, Kanazawa 920-1192, Ishikawa, Japan. Phone: 81-76-264-6270; Fax: 81-76-264-6270; E-mail: katsumi@kenroku.kanazawa-u.ac.jp.

doi:10.1158/0008-5472.CAN-09-0869

MKK6-activated p38α (both isolated from baculovirus-infected Sf21 cells) were obtained from Upstate. Oligonucleotides were synthesized by Invitrogen. The cDNAs and antibodies used in the experiments were described in Supplementary Materials and Methods.

Cell culture and plasmid transfection. HeLa cells were grown in DMEM as previously described (13). Plasmids were transiently transfected with Lipofectamine 2000 (Invitrogen). Cell cycle synchronization was performed using the double thymidine block protocol. To obtain stable Flag-tagged Cdc25B (F-Cdc25B)–expressing HeLa cells, we used 10 μg/mL blasticidin S (Invitrogen) for the selection of transformed cells. Established Flag-Cdc25B–expressing HeLa cells were maintained with 2 μg/mL blasticidin S.

Preparation of crude extracts, immunoblotting, immunoprecipitation, and kinase assay. Crude extracts for the analysis of proteins followed by immunoblotting or immunoprecipitation were performed as described previously (13). To detect endogenous Cdc25B, we subjected proteins that had been immunoprecipitated with rabbit anti-Cdc25B antibodies to SDS-PAGE, followed by immunoblotting. The Cdc25B protein was detected with mouse monoclonal anti-Cdc25B antibody. The immunoprecipitates used for the kinase assay were washed twice with buffer containing 100 mmol/L Tris-HCl (pH 8.0), 5 mmol/L EGTA, and 20 mmol/L $MgCl_2$. The samples were then incubated with the same buffer that was supplemented with appropriate glutathione *S*-transferase (GST) fusion Cdc25B proteins, 1 mmol/L DTT, 200 μmol/L ATP, and [γ-^{32}P]ATP (1 μCi = 37 KBq; Perkin-Elmer). The reaction mixtures were incubated at 30°C for 60 min and subjected to SDS-PAGE, and radioactivity was detected using the Fuji BAS system (Fujifilm).

Indirect immunofluorescence and flow cytometry. Indirect immunofluorescence of cells grown on glass coverslips was conducted as described previously (13). Cells treated for fluorescence-activated cell sorting (FACS) were analyzed on a FACSCalibur (BD Biosciences) using ModFit software. The Ser^{10}-phosphorylated histone H3 (phospho-S10-H3)–positive cells were analyzed using CellQuest software.

Results

Nuclear localization of Cdc25B is lost following treatment of cells with anisomycin but not with DNA-damaging agents. Phosphorylation of Ser^{309} of Cdc25B1 followed by binding of 14-3-3 disrupts nuclear localization of Cdc25B (13). Ser^{309} can be phosphorylated by Chk1/2 and MK2 (18, 25, 26). To determine the types of cellular stresses that induce nuclear export, we treated cells with various chemicals and analyzed the subcellular localization of Cdc25B. Given that an antibody that displayed high specificity toward endogenous Cdc25B was not available commercially or in house, we first established a HeLa cell–based cell line that constitutively expressed F-Cdc25B. No gross abnormality of cell growth or morphology was discerned for F-Cdc25B–expressing cells, which are hereafter called HeLa-W40 cells.

We treated HeLa-W40 cells with hydroxyurea, aphidicolin, etoposide, or camptothecin, which activate either Chk1 or Chk2. DNA damage induced by the chemicals was confirmed by assaying for phosphorylated histone H2AX (γ-H2AX; ref. 27). Cdc25B localized to the nucleus in cells with or without DNA damage or replication arrest (Fig. 1*A*). We next investigated the possible involvement of the p38/MK2 pathways in this process. To activate the p38/MK2 pathway, we treated the cells with anisomycin, which activates p38 and JNK (28, 29). Treatment with anisomycin disrupted the nuclear localization of Cdc25B and promoted the redistribution of Cdc25B to the cytoplasm (Fig. 1*B*). These results suggest that Cdc25B nuclear localization can be disrupted by stress pathways other than those initiated by DNA damage.

To assess the possibility that the p38 pathway regulates Cdc25B, we added the p38 inhibitor SB202190 to HeLa-W40 cells. Of interest

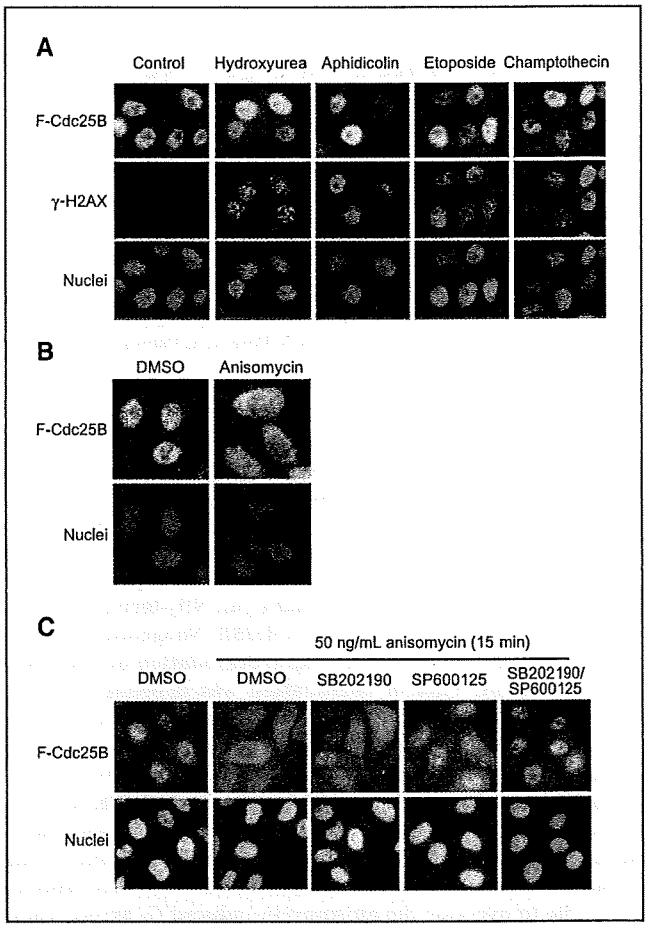

Figure 1. Nuclear localization of Cdc25B is maintained after DNA damage but is disturbed by anisomycin treatment. *A*, HeLa-W40 cells were treated with the indicated chemicals and Flag-Cdc25B and γ-H2AX were detected by indirect immunofluorescence. The nuclei were identified using 4′,6-diamidino-2-phenylindole. The conditions for chemical treatment were described in Supplementary Materials and Methods. *B*, HeLa-W40 cells were treated with 50 ng/mL anisomycin for 15 min and processed for indirect immunofluorescence. *C*, HeLa-W40 cells were pretreated with the indicated MAPK inhibitors for 1 h followed by anisomycin challenge. The cells were fixed, and Flag-Cdc25B and nuclei were analyzed. The concentration for inhibitors was as follows: SB202190, 20 μmol/L; SP600125, 20 μmol/L.

is that SB202190 exerted only a small effect on the anisomycin-induced diffusion of Cdc25B (Fig. 1*C*). In contrast, the JNK inhibitor SP600125 induced strong nuclear staining of Cdc25B under conditions of anisomycin stress. Furthermore, stronger nuclear signals for Cdc25B were generated by simultaneous treatment with both SB202190 and SP600125 than by treatment with SP600125 alone. Inhibition of MAPK/extracellular signal-regulated kinase (ERK) kinase (MEK1) with U0126, thereby inhibiting the activation of ERK1/2, did not prevent cytoplasmic diffusion of Cdc25B (data not shown). Collectively, these data indicate that anisomycin-mediated stress can disrupt nuclear localization of Cdc25B in a JNK-dependent manner.

Cdc25B is degraded in cells treated with anisomycin or sodium chloride but not with DNA-damaging agents. The signals for F-Cdc25B faded in cells after long-term exposure to anisomycin but not after treatment with DNA-damaging agents (data not shown). These observations led us to analyze the level of F-Cdc25B protein in HeLa-W40 cells treated with anisomycin and another

nongenotoxic reagent, sodium chloride (NaCl). We also examined the levels of Cdc25A and Cdc25C to determine whether different cellular stresses affect members of this phosphatase family. Genotoxic stress caused by exposure to hydroxyurea, aphidicolin, etoposide, or camptothecin effectively induced Cdc25A degradation (Fig. 2*A*). In contrast, expression of Cdc25B or Cdc25C was unaffected under the same conditions. Although neither anisomycin nor NaCl activated Chk1 or Chk2, both Cdc25B and Cdc25A were degraded (Fig. 2*A*). Cdc25A and Cdc25B decreased in a time-dependent fashion after exposure to anisomycin (Fig. 2*B*). The endogenous Cdc25B protein in parental HeLa cells was also degraded by anisomycin treatment but not by DNA-damaging agents (Supplementary Fig. S1). The abundance of Cdc25C was not affected by any of the stimuli examined here. UV irradiation, which is known to activate not only Chk1/2 but also p38/JNK, abrogated nuclear localization of Cdc25B as reported (22) and induced Cdc25B degradation (Supplementary Fig. S2*A* and *B*).

Although anisomycin inhibits protein synthesis (29), the more rapid decline of Cdc25B in anisomycin-treated cells compared with cycloheximide-treated cells suggested that degradation of Cdc25B was specifically caused by anisomycin-induced stress and not by a general inhibition of protein synthesis (Fig. 2*C*). More convincing evidence was obtained when we examined the stability of Cdc25B that contained mutations at the constitutive β-TrCP binding site of ^{254}DDGFVD^{259} (amino acid numbering is based on human Cdc25B1; ref. 30). The site is responsible for the steady-state degradation of Cdc25B by a constitutive SCF$^{\beta\text{-TrCP}}$–mediated ubiquitin-proteasome pathway. We established a HeLa cell line expressing a mutant Cdc25B that contained mutations at the β-TrCP binding site (Cdc25B^{DAA}, of which D255 and G256 were replaced by Ala). Figure 2*D* shows that Cdc25B^{DAA} was unstable after anisomycin treatment. This indicates that the Cdc25B degradation was specific to anisomycin treatment. Collectively, these data indicate that anisomycin-induced stress, but not DNA damage–induced stress, triggers a loss of nuclear localization and stability of Cdc25B.

Inhibition of JNK attenuates the degradation of Cdc25B by anisomycin. To determine the role of p38 or JNK on the stability of Cdc25A and Cdc25B, we treated HeLa cells with inhibitors of p38 or JNK and analyzed the cellular proteins. The activation of p38α/β was monitored as the slower migrating form of MK2, corresponding to phosphorylated MK2 (Fig. 3*A*); JNK activation was monitored using antibodies recognizing phospho-JNK1 or phospho–c-Jun. We found that the JNK inhibitor SP600125 protected Cdc25B from anisomycin-induced degradation (Fig. 3*A*, *lanes 5–8*). A relatively small but definite contribution of the p38 pathway to the degradation of Cdc25B was revealed by these experiments (Fig. 3*A*, *lanes 3–8*). The MEK1 inhibitor U0126 again had no effect on the stability of either Cdc25A or Cdc25B (data not shown). Time course experiments further validated the critical role of JNK in regulating the degradation of Cdc25B (Fig. 3*B*). The stability of Cdc25C was essentially unaffected by these inhibitors (Fig. 3*A*). Exactly the same results were obtained with HeLa-W40 cells that expressed F-Cdc25B (Supplementary Fig. S3*A*). JNK inhibitor also attenuated the NaCl-induced F-Cdc25B degradation (Supplementary Fig. S3*B*). Results shown in Fig. 3*C* indicate the correlation between the degradation of Cdc25A/Cdc25B and activation of p38/JNK. Anisomycin-, NaCl-, or UV-induced degradation of Cdc25B was inhibited by the proteasome inhibitor MG132, suggesting that the anisomycin-induced degradation of Cdc25B is mediated by the ubiquitin-proteasome pathway (Supplementary Fig. S3*C*, *1*, *2*, and *3*).

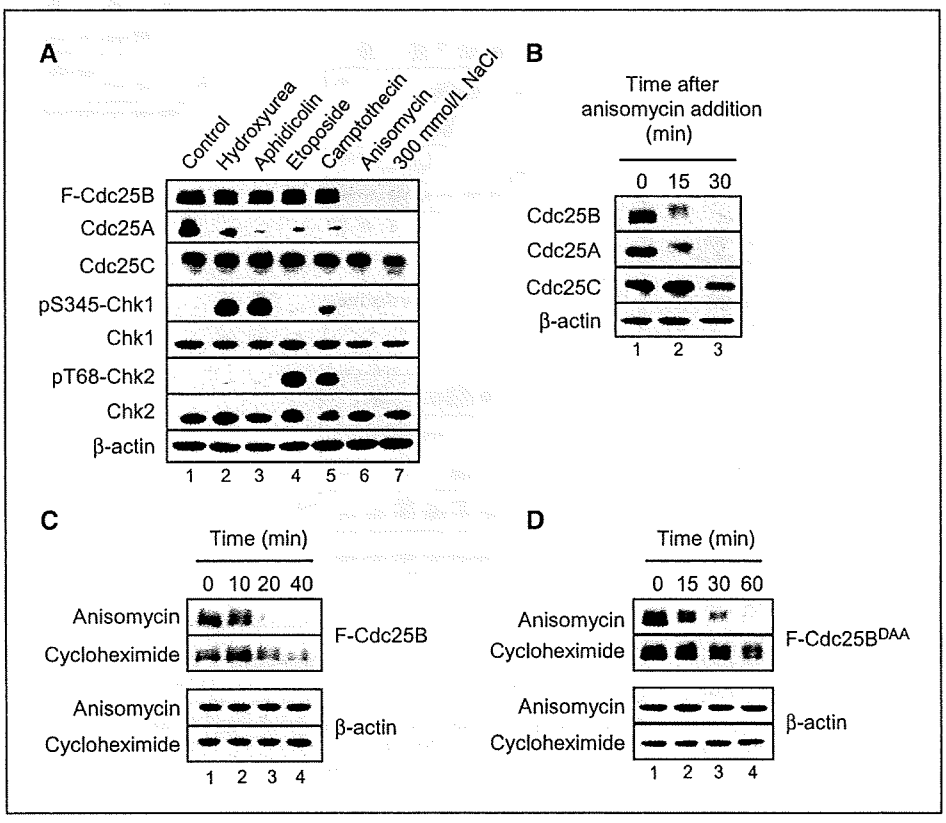

Figure 2. Degradation of Cdc25A and Cdc25B after treatment with DNA-damaging or non–DNA-damaging agents. *A*, HeLa-W40 cells were treated with genotoxic chemicals as described in Supplementary Materials and Methods. The cells were incubated with anisomycin or 300 mmol/L NaCl for 30 min or 1 h, respectively. Cell extracts were prepared, and indicated proteins were detected by immunoblotting. β-Actin analysis serves as a loading control. *B*, parental HeLa cells were treated with anisomycin, and cell extracts were prepared at the indicated time to detect endogenous Cdc25A, Cdc25B, and Cdc25C. *C*, HeLa-W40 cells were treated with anisomycin or 50 μg/mL cycloheximide. Crude extracts were prepared at the indicated time, and the expression of Flag-Cdc25B was analyzed. *D*, HeLa cells constitutively expressing the Cdc25B^{DAA} mutant were treated with anisomycin or cycloheximide and the expression of Flag-Cdc25B proteins was determined by immunoblotting.

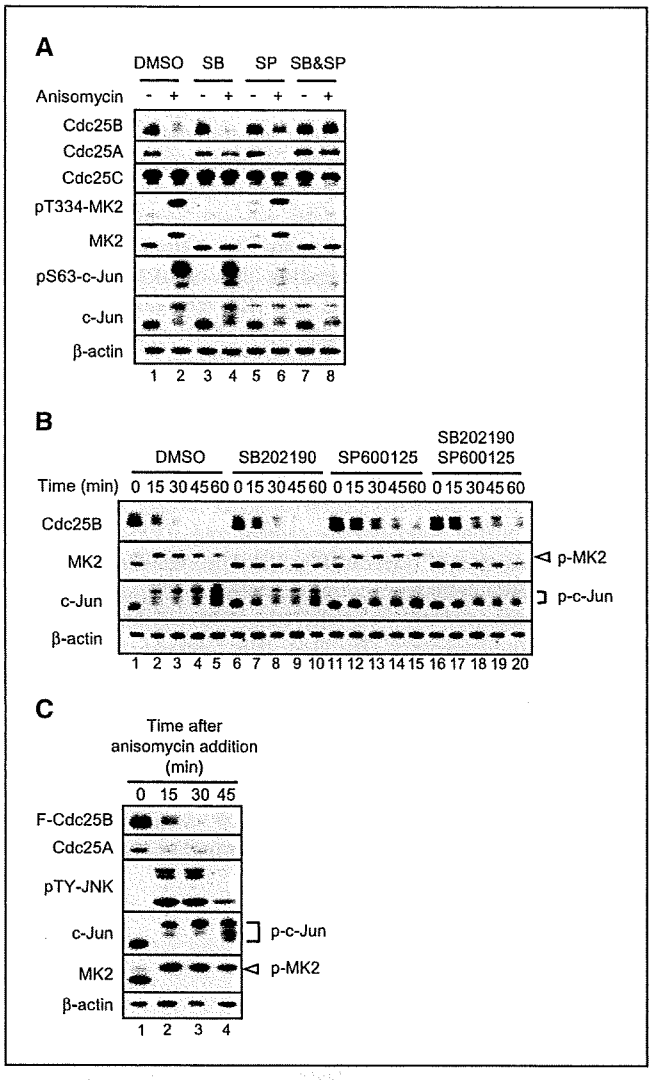

Figure 3. JNK inhibitor SP600125 attenuates the anisomycin-induced Cdc25B degradation. *A*, HeLa cells were treated with the indicated MAPK inhibitors for 1 h followed by anisomycin treatment. Cell extracts were prepared at 20 min after anisomycin addition. *SB*, SB202190; *SP*, SP600125. *B*, HeLa cells were treated with MAPK inhibitors, and the expression of proteins was determined at the indicated time. *C*, HeLa-W40 cells were treated with anisomycin, and the expression of protein was determined at the indicated time. Slower migrating bands of c-Jun and MK2 represent phosphorylated forms of the proteins.

Results of indirect immunofluorescence also supported that the instability of Cdc25B in anisomycin-treated cells was due to its proteasome-dependent degradation (Supplementary Fig. S3*D*).

The coexpression of either JNK1 or JNK2 with MKK7 triggered Cdc25B degradation (Fig. 4*A*). In addition, p38α was able to induce Cdc25B degradation. Furthermore, the expression of kinase-dead JNK1 and JNK2 stabilized Cdc25B (Fig. 4*B*), indicating dominant-negative effects. We further examined the contribution of MK2 to Cdc25B degradation. In this experiment, we used the D316N mutant of p38α, which is unable to activate MK2 (31). As shown in Fig. 4*C*, expression of $p38\alpha^{D316N}$ induced the degradation of Cdc25B. Taken together, these results suggest that JNK and p38 are integrally involved in Cdc25B degradation.

JNK phosphorylates Cdc25B. We found that bacterially expressed Cdc25B was phosphorylated by kinase-active JNK1 but not by its kinase-dead form, indication that JNK1 can directly phosphorylate Cdc25B (Supplementary Fig. S4*A*). Likewise, recombinant JNK1 could also phosphorylate Cdc25B (Supplementary Fig. S4*B*). To identify the phosphorylation site(s) on Cdc25B, GST fusion constructs of different fragments of Cdc25B were produced in *Escherichia coli* and used as substrates for kinase assays. As shown in Fig. 5*A*, JNK phosphorylation sites were present in the NH_2-terminal 175 amino acids. The same fragment was also phosphorylated by recombinant p38α (Supplementary Fig. S4*C*). Furthermore, JNK and Cdc25B were able to form complex, which supports the idea of Cdc25B being a JNK substrate [Supplementary Fig. S5*A*; the loss of the complex formation in wild-type (WT) JNK with MKK7 suggests that JNK may dislodge after phosphorylation event]. The importance of the NH_2-terminal region was also supported by the JNK-induced degradation of the construct containing green fluorescent protein fused to the NH_2-terminal 175 amino acid fragment of Cdc25B (Supplementary Fig. S5*B*).

Cdc25B/S101 is a candidate JNK phosphorylation site. To identify JNK phosphorylation site(s), we first mutated all six candidate serine residues to alanine in six potential JNK substrate SP sequences (and no TP) in N175-Cdc25B. The 6SA mutant was refractory to JNK- or p38α-induced degradation (Supplementary Fig. S6*A*). The coexpression of the individual SA mutant Cdc25B with JNK indicated the importance of S101, followed by S103 (Fig. 5*B*). The importance of S101 and S103 was further supported

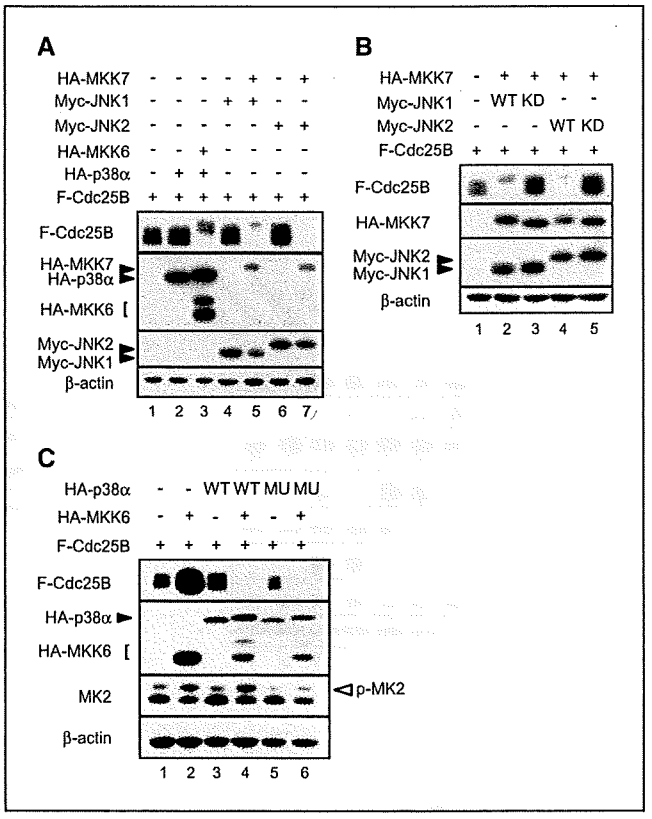

Figure 4. Involvement of JNK in the destabilization of Cdc25B. *A*, HeLa cells were transfected with Flag-Cdc25B in combination with MKK6 and p38α, or MKK7 and JNK1 or JNK2. The expression of the indicated proteins was determined by immunoblotting. *B*, expression of Flag-Cdc25B was determined after cotransfection with MKK7 and either the WT or kinase-dead (*KD*) form of JNK1 or JNK2. *C*, expression of Flag-Cdc25B was examined after cotransfection with MKK6 and WT or the D316N mutant (*MU*) of p38α. *Arrowhead*, phospho-MK2.

by the slower degradation rate of the Cdc25B protein with a double mutation (S101/103A) compared with the mutants with a single mutation (Fig. 5*C*, *lanes 4*, *6*, and *8*). Essentially the same results were obtained when p38α was used as a kinase for the Cdc25B mutants (Supplementary Fig. S6*B*). Taken together, these data indicate that phosphorylation of Cdc25B at S101 and S103 by JNK and p38 is important for degradation.

HeLa cells expressing the Cdc25B S101A mutant ignore anisomycin-induced G_2 arrest. We next examined the effects of anisomycin on cell cycle progression, in particular during G_2-M phase, when Cdc25B peaks during the cell cycle. HeLa cells were synchronized at G_1-S and released into S phase. At 6 hours after release, the cells were treated with anisomycin followed by monitoring of M-phase entry by detection of phospho-S10-H3. Cdc25B and phospho-S10-H3 increased progressively in DMSO-treated cells

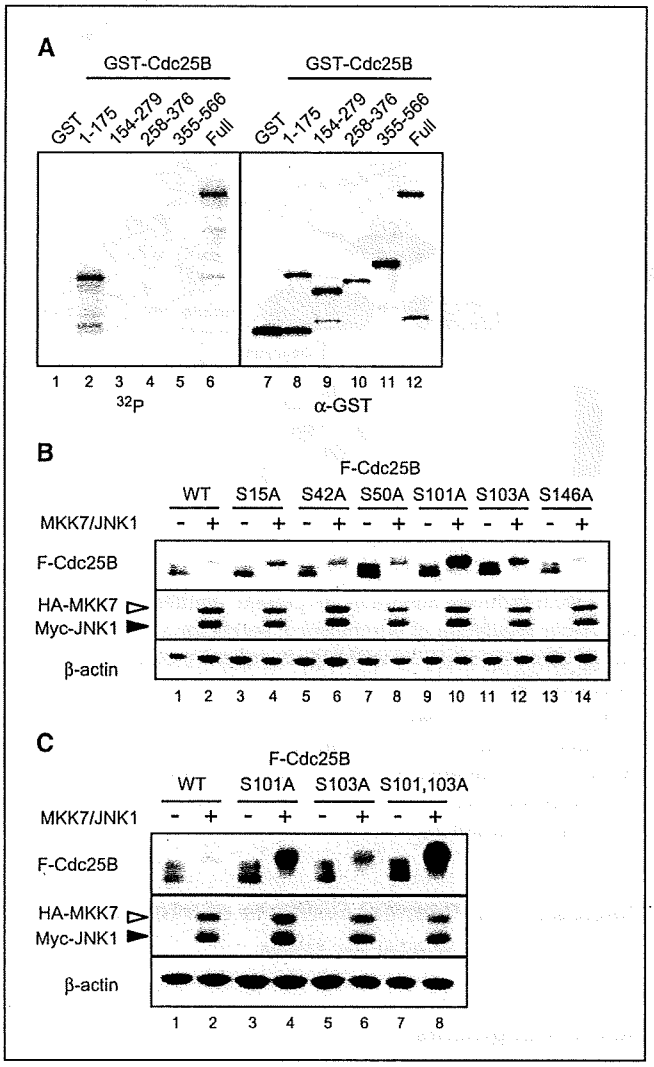

Figure 5. Phosphorylation of Cdc25B by JNK at possible phosphorylation sites. *A*, *left*, GST-Cdc25B fragments were incubated with a recombinant JNK1 in the presence of [γ-^{32}P]ATP followed by autoradiography; *right*, substrate GST-Cdc25B fragment as detected by anti-GST antibody. *B*, WT Cdc25B or mutants that contained SA mutations at candidate JNK phosphorylation sites were cotransfected into HeLa cells with or without MKK7 and JNK1, and expression of Cdc25B was determined by immunoblotting. *C*, the WT or SA mutant at S101, S103, or S101/103 was cotransfected into HeLa cells with or without MKK7 and JNK1, and the expression of Cdc25B was determined.

(Fig. 6*A*), but no phospho-S10-H3 was detected in anisomycin-treated cells, indicating that anisomycin treatment inhibited mitotic entry. In such cells, Cdc25B disappeared completely by 30 minutes after addition of anisomycin (Fig. 6*A*, *lanes 7* and *8*). FACS analysis confirmed the induction of a G_2 delay by anisomycin treatment in synchronously or asynchronously growing HeLa cells (Supplementary Fig. S7*A*).

To delineate the significance of Cdc25B S101 phosphorylation in anisomycin-induced G_2 arrest, we added anisomycin to asynchronously growing HeLa cells that constitutively express the nonphosphorylatable Cdc25B S101A mutant (HeLa-101-1). The results shown in Fig. 6*B* indicate that the half-life of the S101A mutant Cdc25B was twice as long as that of the WT after anisomycin treatment (~35 minutes in S101A and ~15 minutes in WT), indicating that phosphorylation of S101 is essential for proper degradation. Treatment of HeLa-101-1 with either NaCl or UV also supported the idea that S101 is important for stress-induced Cdc25B degradation (Supplementary Fig. S8*A*).

We next investigated whether the S101A mutant would exhibit abrogation of anisomycin-induced G_2 arrest. We used cell lines expressing WT Cdc25B (W40) or S101A (101-1). The amount of Cdc25B protein in W40 cells and that of 101-1 is shown in Supplementary Fig. S7*B*. Asynchronously growing HeLa cells, W40 cells, and 101-1 cells were treated with 100 ng/mL anisomycin, and the number of cells entering M phase during a 3-hour treatment with anisomycin was determined by detecting phospho-S10-H3. As shown in Fig. 6*C*, HeLa-101-1 cells exhibited resistance to anisomycin-induced G_2 retardation. Thus, cells expressing S101A-mutated Cdc25B seem to be more resistant to anisomycin-induced degradation and to recover more rapidly than WT Cdc25B-expressing cells.

Collectively, HeLa cells expressing Cdc25B with a nonphosphorylatable mutation at the possible JNK target S101 residue were more refractory to anisomycin-induced cell cycle retardation.

Discussion

We report here for the first time that Cdc25B is targeted for degradation in cells that are challenged with anisomycin or NaCl and that the degradation of Cdc25B is mediated mainly by JNK. We uncovered this phenomenon by using HeLa cells that constitutively expressed recombinant Cdc25B. In our hands, commercially available antibodies did not properly recognize endogenous Cdc25B in crude extracts by immunoblotting. Immunoprecipitation followed by immunoblotting was necessary to detect endogenous Cdc25B.

Our experiments highlight the critical role of JNK in controlling Cdc25B stability. A level of DNA damage that is sufficient for activating Chk1/2 and Cdc25A degradation did not exert any effects on the stability of Cdc25B. Export of Cdc25B from the nucleus to the cytoplasm is thought to be a mechanism of checkpoint response (18). However, Cdc25B did not follow this expected pattern after DNA damage (Fig. 1*A*). We therefore suspect that Cdc25B is not a primary target of the DNA damage checkpoint, although we cannot exclude the possibility that its phosphatase activity is directly repressed by a Chk1-dependent mechanism (32).

We showed that M-phase entry is delayed in HeLa cells treated with anisomycin (Fig. 6). The G_2 retardation observed in this situation is caused in part by the degradation of Cdc25A and Cdc25B. Depletion of either Cdc25A or Cdc25B is insufficient for G_2-phase arrest, but the depletion of both Cdc25A and Cdc25B is necessary for a more robust G_2 arrest (4). Therefore, anisomycin-induced G_2

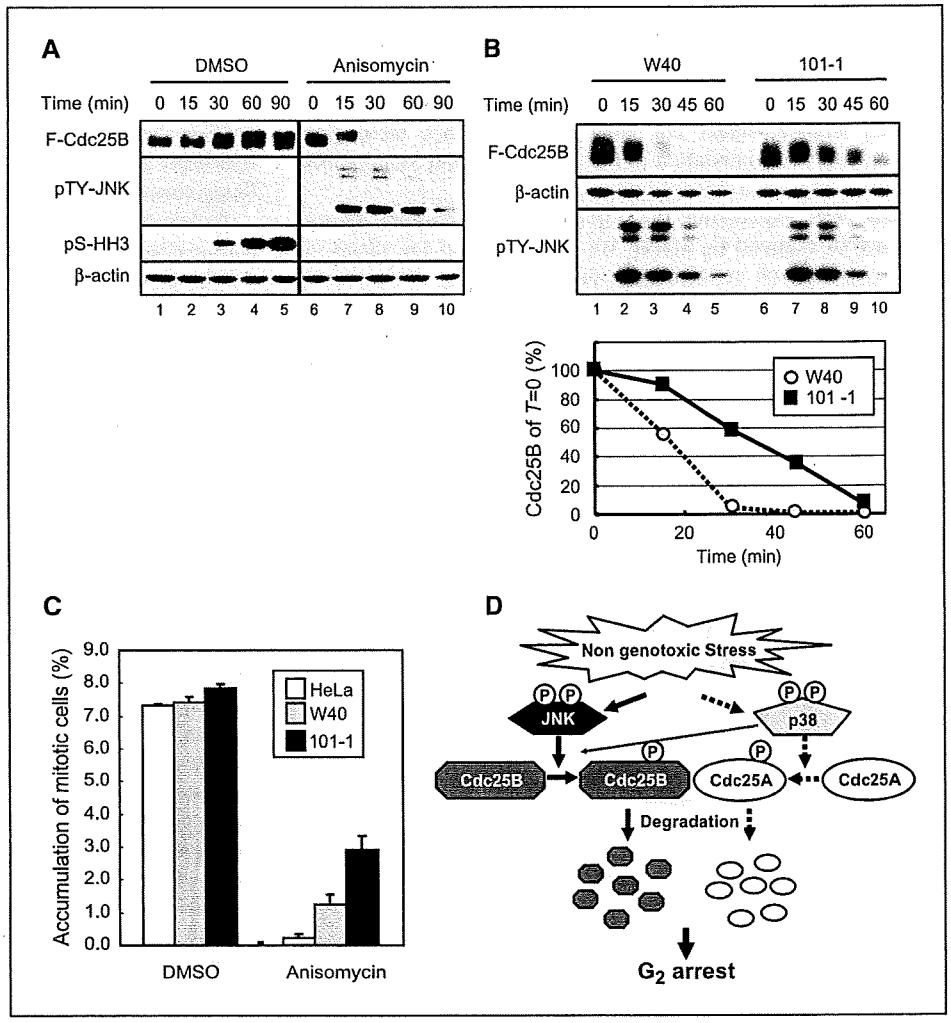

Figure 6. The Cdc25B mutant is refractory to anisomycin-induced G_2 arrest. *A*, HeLa cells synchronized at G_1-S were released into the cell cycle for 6 h, followed by the addition of anisomycin. At the indicated times, the expression of proteins was determined. *B*, HeLa-W40 or HeLa-101-1 cells were treated with anisomycin, and the expression of the proteins was determined at the indicated time points after treatment. *Bottom*, quantitative results. Typical results of three independent experiments are shown. *C*, asynchronously growing HeLa, HeLa-W40, or HeLa-101-1 cells were treated with 100 ng/mL anisomycin and 100 ng/mL nocodazole for 3 h. Cells were collected, and the cells in M phase were determined by detecting phospho-histone H3-Ser^{10} by FACS. *Columns*, mean of three independent experiments; *bars*, SD. The percentage of mitotic cells in asynchronous cells was as follows: HeLa, 2.76 ± 0.27; W40, 3.57 ± 0.13; 101-1, 3.61 ± 0.14. *D*, a model of the induction of Cdc25A and Cdc25B degradation after nongenotoxic stress followed by G_2 arrest.

retardation can be explained at least in part by the simultaneous degradation of Cdc25A and Cdc25B (Fig. 2). Our results strongly suggest the presence of a nongenotoxic stress–dependent cell cycle checkpoint wherein Cdc25 phosphatases are degraded to down-regulate CDK activity. This checkpoint is mediated by stress-activated MAPKs, including p38 and JNK, as depicted in Fig. 6*D*. The proteasome inhibitor MG132 attenuated anisomycin-induced Cdc25B degradation, which strongly suggests that Cdc25B is degraded by the ubiquitin-proteasome pathway. Cdc25B is degraded in the steady state by the $SCF^{\beta\text{-}TrCP}$–mediated ubiquitinylation mechanism. It is unlikely that phosphorylation of S101 stimulated binding of $SCF^{\beta\text{-}TrCP}$ to the constitutive binding site, which is located more than 100 amino acids downstream of S101. It is necessary to identify the responsible ubiquitinylation system to understand JNK-mediated Cdc25B degradation more precisely.

Several reports have indicated a correlation between the malignancy of tumors and the overexpression of Cdc25A and Cdc25B (33, 34). Cdc25A and Cdc25B are oncogenic (35), and Cdc25A is a main target of the DNA damage checkpoint (1, 2, 34). Assuming that Cdc25B is a target of a nongenotoxic stress checkpoint, overexpression of Cdc25B may allow cells to become less sensitive to intrinsically harmful cell stresses that do not directly compromise genome integrity. Ignoring the detrimental stress signal, such as NaCl-induced distortion of the cytoskeleton by hyperosmolarity or anisomycin-induced inhibition of protein synthesis, may disrupt the proper regulation of chromosome segregation and cytokinesis during mitosis, which are well-known causative events of genome instability (36).

In conclusion, we have shown that Cdc25B is targeted for JNK-mediated degradation by cellular stress. The stress-induced checkpoint is initiated by the activation of JNK and p38, which phosphorylates Ser^{101} of Cdc25B. This results in the rapid degradation of Cdc25B and cell cycle arrest.

Disclosure of Potential Conflicts of Interest

No potential conflicts of interest were disclosed.

Acknowledgments

Received 3/6/09; revised 4/22/09; accepted 6/3/09; published OnlineFirst 7/28/09.

Grant support: Long-range Research Initiative of the Japan Chemical Industry Association; Ministry of Health, Labor, and Welfare of Japan; Japan Society for the Promotion of Science; and Yamagiwa-Yoshida Fellowship from the International Union Against Cancer, Switzerland.

The costs of publication of this article were defrayed in part by the payment of page charges. This article must therefore be hereby marked *advertisement* in accordance with 18 U.S.C. Section 1734 solely to indicate this fact.

We thank Dr. H. Shima for the p38α plasmid and Dr. M. Ogata for information on the *sevenmaker* mutation of MAPKs.

References

1. Bartek J, Lukas J. Mammalian G_1- and S-phase checkpoints in response to DNA damage. Curr Opin Cell Biol 2001;13:738–47.
2. Busino L, Chiesa M, Draetta GF, Donzelli M. Cdc25A phosphatase: combinatorial phosphorylation ubiquitylation and proteolysis. Oncogene 2004;23:2050–6.
3. Mailand N, Podtelejnikov AV, Groth A, Mann M, Bartek J, Lukas J. Regulation of G_2/M events by Cdc25A through phosphorylation-dependent modulation of its stability. EMBO J 2002;21:5911–20.
4. Lindqvist A, Källström H, Lundgren A, Barsoum E, Rosenthal CK. Cdc25B cooperates with Cdc25A to induce mitosis but has a unique role in activating cyclin B1-Cdk1 at the centrosome. J Cell Biol 2005;171:35–45.
5. Bartek J, Lukas J. Chk1 and Chk2 kinases in checkpoint control and cancer. Cancer Cell 2003;3:421–9.
6. Jin J, Shirogane T, Xu L, et al. $SCF^{\beta\text{-}TRCP}$ links Chk1 signaling to degradation of the Cdc25A protein phosphatase. Genes Dev 2003;17:3062–74.
7. Chen MS, Hurov J, White LS, Woodford-Thomas T, Piwnica-Worms H. Absence of apparent phenotype in mice lacking Cdc25C protein phosphatase. Mol Cell Biol 2001;21:3853–61.
8. Ferguson AM, White LS, Donovan PJ, Piwnica-Worms H. Normal cell cycle and checkpoint responses in mice and cells lacking Cdc25B and Cdc25C protein phosphatases. Mol Cell Biol 2005;25:2853–60.
9. Lincoln AJ, Wickramasinghe D, Stein P, et al. Cdc25b phosphatase is required for resumption of meiosis during oocyte maturation. Nat Genet 2002;30:446–9.
10. Dutertre S, Cazales M, Quaranta M, et al. Phosphorylation of CDC25B by Aurora-A at the centrosome contributes to the G_2-M transition. J Cell Sci 2004;117:2523–31.
11. Kramer A, Mailand N, Lukas C, et al. Centrosome-associated Chk1 prevents premature activation of cyclin-B-Cdk1 kinase. Nat Cell Biol 2004;6:884–91.
12. Schmitt E, Boutros R, Froment C, Monsarrat B, Ducommun B, Dozier C. CHK1 phosphorylates CDC25B during the cell cycle in the absence of DNA damage. J Cell Sci 2006;119:4269–75.
13. Uchida S, Kuma A, Ohtsubo M, et al. Binding of 14-3-3β but not 14-3-3σ controls the cytoplasmic localization of CDC25B: binding site preferences of 14-3-3 subtypes and the subcellular localization of CDC25B. J Cell Sci 2004;117:3011–20.
14. Boutros R, Dozier C, Ducommun B. The when and where of CDC25 phosphatases. Curr Opin Cell Biol 2006;18:185–91.
15. Forrest A, Gabrielli B. Cdc25B activity is regulated by 14-3-3. Oncogene 2001;20:4393–401.
16. Davezac N, Baldin V, Gabrielli B, et al. Regulation of CDC25B phosphatases subcellular localization. Oncogene 2000;19:2179–85.
17. Johnson GL, Lapadat R. Mitogen-activated protein kinase pathways mediated by ERK JNK and p38 protein kinases. Science 2002;298:1911–2.
18. Manke IA, Nguyen A, Lim D, Stewart MQ, Elia AE, Yaffe MB. MAPKAP kinase-2 is a cell cycle checkpoint kinase that regulates the G_2/M transition and S phase progression in response to UV irradiation. Mol Cell 2005;17:37–48.
19. Bulavin DV, Amundson SA, Fornace AJ. p38 and Chk1 kinases: different conductors for the G_2/M checkpoint symphony. Curr Opin Genet Dev 2002;12:92–7.
20. Goloudina A, Yamaguchi H, Chervyakova DB, Appella E, Fornace AJ, Jr., Bulavin DV. Regulation of human Cdc25A stability by serine 75 phosphorylation is not sufficient to activate an S phase checkpoint. Cell Cycle 2003;2:473–8.
21. Goss VL, Cross JV, Ma K, Qian Y, Mola PW, Templeton DJ. SAPK/JNK regulates cdc2/cyclin B kinase through phosphorylation and inhibition of cdc25C. Cell Signal 2003;15:709–18.
22. Lindqvist A, Källström H, Karlsson-Rosenthal C. Characterisation of Cdc25B localisation and nuclear export during the cell cycle and in response to stress. J Cell Sci 2004;117:4979–90.
23. Uchida S, Ohtsubo M, Shimura M, et al. Nuclear export signal in CDC25B. Biochem Biophys Res Commun 2004;316:226–32.
24. Uchida S, Kubo A, Kizu R, et al. Amino acids C-terminal to the 14-3-3 binding motif in CDC25B affect the efficiency of 14-3-3 binding. J Biochem (Tokyo) 2006;139:761–9.
25. Bulavin DV, Higashimoto Y, Popoff IJ, et al. Initiation of a G_2/M checkpoint after ultraviolet radiation requires p38 kinase. Nature 2001;411:102–7.
26. Lemaire M, Froment C, Boutros R, et al. CDC25B phosphorylation by p38 and MK-2. Cell Cycle 2006;5:1649–53.
27. Rogakou EP, Pilch DR, Orr AH, Ivanova VS, Bonner WM. DNA double-stranded breaks induce histone H2AX phosphorylation on serine 139. J Biol Chem 1998;273:5858–68.
28. Cano E, Hazzalin CA, Mahadevan LC. Anisomycin-activated protein kinases p45 and p55 but not mitogen-activated protein kinases ERK-1 and -2 are implicated in the induction of c-fos and c-jun. Mol Cell Biol 1994;14:7352–62.
29. Iordanov MS, Pribnow D, Magun JL, et al. Ribotoxic stress response: activation of the stress-activated protein kinase JNK1 by inhibitors of the peptidyl transferase reaction and by sequence-specific RNA damage to the α-sarcin/ricin loop in the 28S rRNA. Mol Cell Biol 1997;17:3373–81.
30. Kanemori Y, Uto K, Sagata N. β-TrCP recognizes a previously undescribed nonphosphorylated destruction motif in Cdc25A and Cdc25B phosphatases. Proc Natl Acad Sci U S A 2005;102:6279–84.
31. Hutter D, Chen O, Barnes J, Liu Y. Catalytic activation of mitogen-activated protein (MAP) kinase phosphatase-1 by binding to p38 MAP kinase: critical role of the p38 C-terminal domain in its negative regulation. Biochem J 2000;352:155–63.
32. Uto K, Inoue D, Shimuta K, Nakajo N, Sagata N. Chk1 but not Chk2 inhibits Cdc25 phosphatases by a novel common mechanism. EMBO J 2004;23:3386–96.
33. Kristjánsdóttir K, Rudolph J. Cdc25 phosphatases and cancer. Chem Biol 2004;11:1043–51.
34. Boutros R, Lobjois J, Ducommun B. CDC25 phosphatases in cancer cells: key players? Good targets? Nat Rev Cancer 2007;7:495–507.
35. Galaktionov K, Lee AK, Eckstein J, et al. CDC25 phosphatases as potential human oncogenes. Science 1995;269:1575–7.
36. Kops GJ, Weaver BA, Cleveland DW. On the road to cancer: aneuploidy and the mitotic checkpoint. Nat Rev Cancer 2005;5:773–85.

Poly(ADP-ribose) Glycohydrolase Deficiency Sensitizes Mouse ES Cells to DNA Damaging Agents

H. Fujihara[1,2,3], H. Ogino[1,2], D. Maeda[1,2], H. Shirai[1], T. Nozaki[1], N. Kamada[4], K. Jishage[4], S. Tanuma[5], T. Takato[3], T. Ochiya[6], T. Sugimura[1] and M. Masutani*[,1,2]

[1]*Biochemistry Division, National Cancer Center Research Institute, 5-1-1, Tsukiji, Chuo-ku, Tokyo 104-0045, Japan;* [2]*ADP-ribosylation in Oncology Project, 5-1-1, Tsukiji, Chuo-ku, Tokyo 104-0045, Japan;* [3]*Department of Oral and Maxillo-facial Surgery, Faculty of Medicine, The University of Tokyo, 7-3-1, Hongo, Bunkyo-ku, Tokyo 113-8655, Japan;* [4]*Chugai Research Institute for Medical Science, Inc., 1-135, Komakado, Gotemba, Shizuoka 412-8513, Japan;* [5]*Department of Biochemistry, Faculty of Pharmaceutical Sciences, Tokyo University of Science, 2641, Yamazaki, Noda City, Chiba 278-8510, Japan;* [6]*Section for Studies on Metastasis, National Cancer Center Research Institute, 5-1-1, Tsukiji, Chuo-ku, Tokyo 104-0045, Japan*

Abstract: Poly(ADP-ribose) glycohydrolase (Parg) is the main enzyme for degradation of poly(ADP-ribose) by splitting ribose-ribose bonds. *Parg*-deficient (*Parg*$^{+/-}$ and *Parg*$^{-/-}$) mouse ES cell lines have been established by disrupting both alleles of *Parg* exon 1 through gene-targeting. A transcript encoding a full length isoform of Parg was eliminated and only low amounts of Parg isoforms were detected in *Parg*$^{-/-}$ embryonic stem (ES) cells. Poly(ADP-ribose) degradation activity was decreased to one-tenth of that in *Parg*$^{+/+}$ ES cells. *Parg*$^{-/-}$ ES cells exhibited the same growth rate as *Parg*$^{+/+}$ ES cells in culture. Sensitivity of *Parg*$^{-/-}$ ES cells to various DNA damaging agents, including an alkylating agent dimethyl sulfate, cisplatin, gemcitabine, 5-fluorouracil, camptothecin, and γ-irradiation was examined by clonogenic survival assay. *Parg*$^{-/-}$ ES cells showed enhanced lethality after treatment with dimethyl sulfate, cisplatin and γ-irradiation compared with wild-type (*Parg*$^{+/+}$) ES cells ($p<0.05$, respectively). In contrast, a sensitization effect by *Parg*-deficiency was not observed with gemcitabine and camptothecin. These results suggest the possibility that functional inhibition of Parg leads to sensitization of tumor cells to some chemo- and radiation therapies.

Keywords: Poly(ADP-ribose) glycohydrolase, Knockout, ES cell, DNA damaging agent, Alkylating agent, γ-irradiation, cisplatin, 5-fluorouracil.

INTRODUCTION

Poly(ADP-ribose) glycohydrolase (Parg) [1], phosphodiesterase and ADP-ribosyl protein lyase [2, 3] are the three main groups of enzymes reported to be involved in poly(ADP-ribose) degradation. Parg specifically degrades poly(ADP-ribose) synthesized by poly(ADP-ribose) polymerase (Parp) family proteins into ADP-ribose through cleavage of the α(1''-2')glycosidic linkage [1]. Recently, an ADP-ribose-(arginine) protein hydrolase (ARH) 1 homolog, ARH3, has been identified to possess Parg activity [4]. Accumulating evidence indicates that Parg is the major enzyme for poly(ADP-ribose) degradation in cells. Poly(ADP-ribose) is suggested to promote repair DNA synthesis [5, 6].

Extensive studies suggest that inhibition of Parp-1 activity causes a sensitization effect to various types of DNA damaging agents, including alkylating agents, topoisomerase I inhibitors and γ-irradiation. Augmented sensitivity to DNA damaging agents could be explained by blockade of DNA repair pathways, including base excision repair and DNA strand break repair pathways [7, 8]. Potent Parp inhibitors are now in clinical trials to test their sensitizing effects for chemotherapeutic agents, including an alkylating agent, temozolomide, or γ-irradiation on cancers [9, 10].

*Address correspondence to this author at the Biochemistry Division, 5-1-1, Tsukiji, Chuo-ku, Tokyo 104-0045, Japan; Fax: +81-3-3542-2530; E-mail: mmasutan@ncc.go.jp

The proper equilibrium of poly(ADP-ribose) synthesis and its degradation may be required in DNA damage response. Inhibition of Parg activity is expected to result in accumulation of polyADP-ribosylated proteins and inactivation or functional alteration of these proteins, which may critically affect DNA damage response. In fact, some studies show that Parg inhibition sensitizes cells to DNA damaging agents. For example, *Parg* knockout mice disrupted at exons 2-3, lacking a full length 110 kDa isoform and expressing a mitochondrial 60 kDa isoform, showed an increased sensitivity to an alkylating agent and γ-irradiation [11]. *Parg*$^{-/-}$ mice lacking all isoforms exhibited early embryonic lethality and *Parg*$^{-/-}$ cells showed increased sensitivity to an alkylating agent and menadione [12]. Although *PARG* knockdown in human cancer cell lines and mouse embryonic fibroblasts showed protection of the cells from acute toxicity by hydrogen peroxide [13], another study reported that *PARG* knockdown in human cancer cells using siRNA resulted in decreased clonogenic survival after treatment with hydrogen peroxide [6].

Parg inhibitor *N*-bis-(3-phenyl-propyl)9-oxo-fluorene-2, 7-diamide augmented the anti-tumor effect of an alkylating agent, temozolomide, in a malignant melamoma model in mice [14]. This study is encouraging for the application of Parg pharmacological inhibition in sensitization to cancer chemotherapy. A previous study showed that Parg inhibitory compounds, gallotannin and nobotannin B, suppressed oxidative and excitotoxic neuronal cell death by preventing NAD depletion and suggested that Parg is positively in-

1568-0096/09 $55.00+.00

volved in the Parp-1-mediated cell death pathway [15]. Mono-galloyl glucose derivatives is reported to inhibit Parg and potentially reduces *N*-methyl-*N*-nitro-*N*-nitrosoguanidine-induced cell death [16]. The effect of Parg inhibition on the action of various types of DNA damaging agents needs to be studied in different cell types to examine the benefit of Parg inhibition in chemo- or radiotherapies of cancer.

In the present study, we established hypomorphic *Parg*-deficient ($Parg^{-/-}$) mouse embryonic stem (ES) cell lines by gene-targeting. Poly(ADP-ribose) degradation activity is reduced to approximately one-tenth in $Parg^{-/-}$ ES cells compared to $Parg^{+/+}$ ES cells. Mouse ES cells are tumorigenic and retain properties similar to teratocarcinoma cells [17]. The sensitivity spectrum in ES cells should be therefore useful to evaluate the impact of Parg functional inhibition in the sensitivity of cancer cells to DNA damaging agents and chemotherapeutic agents. Here in this study, $Parg^{-/-}$ ES cells showed increased sensitivity to different types of DNA damaging agents including a monofunctional alkylating agent, dimethyl sulfate (DMS), cisplatin and γ-irradiation. Early and augmented formation of an oligonucleosomal DNA ladder after treatment with DMS in $Parg^{-/-}$ ES cells suggests that the apoptotic cell death process is accelerated under *Parg* deficiency. The findings suggest that Parg inhibition is useful for sensitization of cancer cells to particular types of chemotherapeutic agents as well as radiotherapy.

MATERIALS & METHODS

Generation of $Parg^{+/-}$ and $Parg^{-/-}$ ES Cell Lines

Mouse *Parg* genomic fragments were isolated by screening a 129Sv mouse BAC library using a mouse *Parg* cDNA fragment as the probe. The targeting vector was constructed as follows; a 7 kb *Eco*RV-*Xho*I fragment spanning *Parg* exon 1 was subcloned into pBlueScript with a negative selection marker, a *diphtheria toxin A* gene (*DT-A*) fragment. An N-terminal 86 bp fragment of the *β-galactosidase* gene (*lacZ*) was prepared by PCR reaction using a sense primer containing *Hin*dIII and *Nar*I sites, 5'-ACTCAGAAGCTT GGCGCCGTCGTTTTAC AACGTCGT G-3', corresponding to nucleotides 708-728 of pSV-β-gal (GenBank accession number: X65335), and an anti-sense primer, 5'-ATGGGATAGGTTACGTTG GTGTA G-3', corresponding to nucleotides 982-1005. The PCR fragment was digested with *Hin*dIII and *Eco*81I and inserted into *Hin*dIII-*Eco*81I digested pSV-β-gal (Promega) and thereby the *Nar*I site was introduced into the *lacZ* gene. A neo^r cassette (a neomycin-resistance gene driven by the MC1 promoter with SV40-derived polyadenylation signal at the 3'-terminus) from pMC1neopolyA was inserted into the *Bam*HI site downstream of the above modified *lacZ* gene and a plasmid containing the neo^r cassette flanked by the mutated *lacZ* and a *loxP* sequence was generated. The 4.5 kb fragment harboring *lacZ/loxP/*neo^r was obtained from this plasmid by *Nar*I digestion. The 4.5 kb fragment harboring *lacZ/loxP/*neo^r was inserted into the *Nar*I site 47 bases downstream of the first ATG in the *Parg* gene in the same orientation as transcription. This *lacZ/loxP/*neo^r targeting vector allowed the in-frame fusion of the *lacZ* gene to *Parg* exon 1, 47 bases downstream of the translation initiation site. In addition, another targeting vector was constructed for the disruption of the remaining allele of the *Parg* gene using a puromycin resistance gene ($puro^r$) cassette [18], kindly donated by Dr. P. Laird. This 13 kb plasmid harbors the 7 kb *Eco*RV-*Xho*I fragment and the *DT-A* gene cassette as above, with replacement of the 0.4 kb *Nar*I fragment containing the first ATG with a *loxP/*$puro^r$ fragment. The neo^r targeting vector was linearized at the *Kpn*I site, electroporated into J1 ES cells, and then ES cells were cultured on a STO cell feeder layer in a medium [19] supplemented with 175 μg/ml G418 (GIBCO/BRL). The STO cells were kindly donated by Dr. P. Laird and STO feeder layer was prepared by treatment with 10 μg/ml mitomycin C (Sigma) for 3 hrs and washing the cells with phosphate-buffered saline (PBS) a for three times. G418-resistant clones were screened by Southern blot analysis to identify $Parg^{+/-}$ ES clones. To generate $Parg^{-/-}$ ES cell clones, $Parg^{+/-}$ ES cell clones were electroporated with the linearized $puro^r$ targeting vector. Selection was performed by culture in the presence of 0.5-1.0 μg/ml of puromycin (Sigma) and 175 μg/ml of G418.

To examine homologous recombination, Southern blot analysis was carried out using the "3'-probe" and "5'-probe", generated as follows. For the "3'-probe", a 264 bp fragment corresponding to exon 3 was prepared by PCR using a sense primer 5'-GACTCCATGATGAGTTCTGTGC-3' and an anti-sense primer 5'-ATCAGTGTGGGGTGACTGACC-3'. This fragment was hybridized to *Bam*HI-digested genomic DNA. For the "5'-probe", a 0.7 kb *Hin*dIII-*Pst*I fragment (see Fig. **1A**), was hybridized to the genomic DNA digested with *Pst*I.

To sequence the targeting junction present in intron 1 of *Timm23 (translocase of inner mitochondrial membrane 23 homolog)* gene, two primers (5'-CAGACTTCCAATTGTT ACACAAGCATC-3' and 5'-GGTCAGTTTGTC TTTAGA GTTGCAAG-3') were used to amplify the DNA fragment, and the fragment was directly sequenced using these primers. To sequence the boundary of the *Timm23* and *Parg* genes, the primers in intron 1 of the *Timm23* gene (5' -CTGTCCAGGAAGGAGTCAG-3') and in exon 1a/exon1 of *Parg* gene (5' -CCTCATTCACTAACCCGGACA-3') were used for the neo^r-allele. The above primer for intron 1 of the *Timm23* gene (5'-CAGACTTCCAATTGT TACACA AGCATC-3') and a primer for the promoter of $puro^r$ (5'-GCTGCTA AAGCGCATGCTCC-3') were used for the $puro^r$ allele.

Northern Blot and RT-PCR Analysis

Northern blot analysis of the *Parg* gene was performed using a 0.2 kbp C-terminal fragment of *Parg* cDNA using total RNA.

For RT-PCR, we used the first-strand cDNA synthesized for 5'RACE RT-PCR, and amplified using LA *Taq* with GC II buffer (TAKARA). Primer sets used to amplify specific sequences were 5'-TGCGGGTCCCAGCATGAGTGCG-3' (S1) and 5'- GAACACGCCTCTGCCTGCC-3' (A3); 5'-CGCTCCCGTCC AGTTCAGG-3' (S2) and 5'-TCTTG GGTCCTTTAGTATCCATCC-3'(A1). The primer set for amplifying *Timm23* was 5'-CAAGGAGCACTTTGGGC

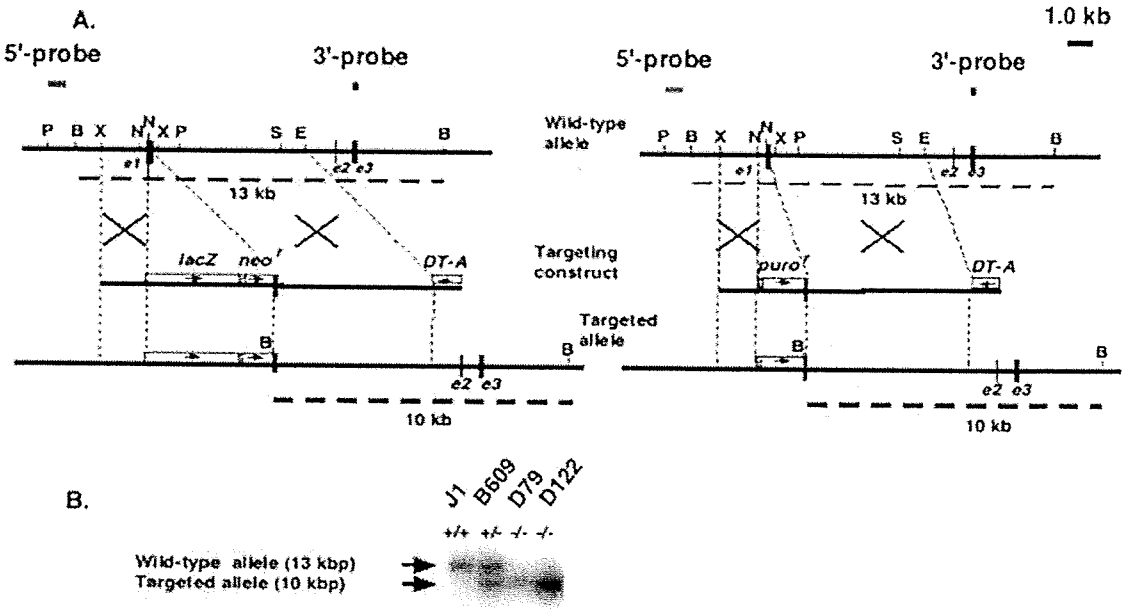

Fig. (1). *Parg* gene-disruption in mouse ES cells. **A.** Gene-targeting strategy. The top lines represent the approximately 18 kb *Parg* genomic locus. The 3'-and 5'-recombination junction probes (3'-probe and 5'-probe, respectively) used to detect the disrupted alleles are shown as solid bars. The locations of restriction enzymes are also shown (N, *Nar*I; E, *Eco*RV; P, *Pst*I; X, *Xho*I; S, *Sac*I, B, *Bam*HI). The middle lines represent the targeting constructs and the positions of the selection marker genes. The sequence of *loxP* is depicted as slashed boxes. Linearization of *puro*^{r} vector with *Sac*I digestion resulted in separation of the *DT-A* cassette from the *Parg* gene sequence, however, *Parg*$^{-/-}$ ES cell clones were obtained at an expected frequency. **B.** Southern blot analysis of *Parg*$^{+/+}$, *Parg*$^{+/-}$ and two *Parg*$^{-/-}$ ES cell clones, D79 and D122. Hybridization with the 3'-probe was performed after digestion of genomic DNAs with *Bam*HI. Gene-disruption was also confirmed by Southern blot analysis using 5'-probe (data not shown).

TAATAC-3' and 5'-ATACAGTGCATAGAGACTGG-3'. PCR products were separated by electrophoresis and visualized by staining with ethidium bromide.

Poly(ADP-Ribose) Degradation and Parg Activity Measurement

ES cell lysate was prepared by suspending cells in a lysis buffer consisting of 20 mM potassium phosphate (pH 7.5), 2 mM EDTA, 10 mM β-mercaptoethanol, 0.1% Triton X-100 containing protease inhibitor cocktail (Complete^{TM}, Roche Diagnostics) and mixed in a blender at 4 °C for 30 min. After centrifugation at 18,000*g* at 4 °C for 15 min, the supernatant was taken and protein quantification was carried out. ^{32}P-Poly(ADP-ribose) was prepared using crude extract from *E. coli* overexpressing human PARP-1, as described [20, 21]. ^{32}P-Poly(ADP-ribose) was detached from the protein and further purified using anionic-exchange column chromatography. ^{32}P-Poly(ADP-ribose) was added at 5 μM (calculated as the ADP-ribose concentration) to the reaction mixture containing 20 mM potassium phosphate (pH 7.5), 2 mM EDTA, 10 mM β-mercaptoethanol, 0.1% Triton X-100, and the crude extracts of ES cells, incubated at 25 °C for 10 min. The aliquot was also used to measure the degradation activity of ^{32}P-poly(ADP-ribose) into ^{32}P-(ADP-ribose) by polyethyleneimine-impregnated cellulose TLC (thin-layer chromatography) plate (Macherey-Nagel) using a developing solvent consisting 3 M acetic acid, 0.1M LiCl and 3 M Urea, as described [20] and the TLC plates were analyzed by BAS2500 (Fuji Film) and the radioactivity of degradation products and the remaining poly(ADP-ribose) was quantified.

Clonogenic Survival Assay

Clonogenic survival assay of ES cells were carried out as described [22, 23]. ES cells were inoculated in triplicate onto 6-well plates (Iwaki) with a STO cell feeder layer as described earlier. Cells were exposed to dimethyl sulfate (DMS, Sigma), cisplatin (Sigma), and hydrogen peroxide (Mitsubishi-Gas Chemicals), gemcitabine (Sigma), camptothecin (Sigma), and 5-fluorouracil (Sigma) at various concentrations for 16 hrs, rinsed two times in PBS and allowed to grow for 8 days. The numbers of ES cells inoculated per well were adjusted to yield at least several colonies on each plate, respectively, and ranged from 500 to 5 x 10^5 cells depending on the chemicals and their concentration or irradiation dose [24]. For γ-irradiation, trypsinized cells were irradiated using a ^{60}Co γ-irradiator at 0.29 Gy/sec, inoculated on a STO cell feeder layer and were left to grow for 8 days as above. The colonies were stained with crystal violet for counting. The clonogenic survival ratio to the untreated control was calculated as follows.

Plating efficiency (P. E.)= (No. of colonies)/(number of inoculated cells)

The clonogenic survival ratio to the untreated control= (P. E. at a given concentration of chemical or irradiation dose)/ (P. E. of untreated cells).

Western Blot Analysis

After sonication and separation by SDS-polyacrylamide gel electrophoresis, proteins were transferred onto Immobilon membranes (Millipore), the membrane was incubated with anti-α-tubulin (1:1,000, ICN Biomedicals), immune complexes were visualized using a horseradish peroxidase-linked secondary antibody and the enhanced chemiluminescence reaction (ECL Plus kit, Amersham). Detection of Timm23 protein was carried out using a monoclonal antibody against Timm23 (BD Bioscience Clontech) diluted at 1:2,500 as above. For detection of Parg, the anti-Parg mouse monoclonal antibody raised against a peptide from the C-terminal half of Parg and horseradish peroxidase-conjugated anti-mouse IgG were diluted with an immunoreaction enhancer solution, Can Get Signal™ (TOYOBO), and incubated with an anti-Parg monoclonal antibody (1:250) for 1 hr and horseradish peroxidase-conjugated anti-mouse IgG (1:5,000) for 1 hr.

Statistical Analysis

Statistical analysis was carried out by Mann-Whitney *U* tests using SPSS software (Macintosh version, SPSS, Chicago) or JMP 5.1.2 (SAS Institute, Cary).

RESULTS

Generation of *Parg*$^{-/-}$ ES Cell Lines Lacking a Full Length Isoform

The *loxP/lacZ/neo*^{r} targeting vector allowed in-frame fusion of the *Parg* gene with *lacZ* at 47 bases downstream of the translation-initiation site in exon 1, and the insertion of the *loxP*-franked *neo*^{r} cassette downstream of the *lacZ* gene in the same orientation to *Parg* transcription, as shown in Fig. (**1A**). After electroporation into J1 ES cells, G418-resistant colonies were isolated and 4 of 704 clones were identified as *Parg*$^{+/-}$ ES cell clones by Southern blot analysis Fig. (**1B**). Disruption of the remaining allele with the *puro*^{r} targeting vector was performed on clone B609, and 6 of 230 *neo*^{r} and *puro*^{r} clones were identified to be *Parg*$^{-/-}$. Representative results of Southern blot analysis are presented as Fig. (**1B**). Two *Parg*$^{-/-}$ ES cell clones, D79 and D122, were employed for further analyses.

Northern blot analysis revealed that the amount of 4 kb *Parg* mRNA in *Parg*$^{-/-}$ ES cells was reduced approximately to one-sixth of that in *Parg*$^{+/+}$ ES cells (Fig. **2A**). Cortes et al. reported that besides a full length *Parg* mRNA (variant 1) containing exons 1a, 1 and 2, a splice variant (variant 2), which lacks exon 1 but harbors exons 1a and 2, is present [11]. RT-PCR analysis using three primer sets specific for *Parg* mRNA (Fig. **2B**) suggested that residual Parg transcripts present in *Parg*$^{-/-}$ ES cells correspond to variant 2 or truncated *Parg* mRNA possessing a second ATG colon present in exon 2. As shown in Fig. (**2C**) (marked with asterisk), western blot analysis revealed that the largest Parg isoform of around 128 kDa, which may correspond to the full length form, was lost in *Parg*$^{-/-}$ ES cell lines and the amounts of the two major isoforms of around 107 kDa and 63 kDa (marked with arrows) in *Parg*$^{-/-}$ ES cell clones were reduced. Although other minor isoforms of 86, 78 and 59 kDa were not observed in *Parg*$^{-/-}$ ES cell clones by western blot analysis, we could not conclude whether these 86, 78 and 59 kDa minor isoforms were absent or present at reduced amounts in *Parg*$^{-/-}$ ES cell clones. The degradation activity of ^{32}P-poly(ADP-ribose) in ES cell extracts was reduced approximately to one-tenth in *Parg*$^{-/-}$ ES cell clones compared with *Parg*$^{+/+}$ ES cell clones (Fig. **2D** and **2E**). A major degradation product was ADP-ribose for both *Parg*$^{+/+}$ and *Parg*$^{-/-}$ ES cells, indicating that degradation to ADP-ribose by Parg is the main degradation pathway in ES cells.

The *Parg* gene shares a putative promoter with the *Timm23* gene [25]. RT-PCR analysis showed that *Timm23* expression level in *Parg*$^{-/-}$ ES cells did not change compared to *Parg*$^{+/+}$ ES cells (Fig. **2F**). Western blot analysis showed that the amount of Timm23 protein in *Parg*$^{-/-}$ ES cells is comparable to that of the *Parg*$^{+/+}$ ES cells (Fig. **2G**). Expression of fused *lacZ* mRNA driven from the *Parg* promoter in a *neo*^{r} allele was detected in *Parg*$^{-/-}$ ES cell clones by RT-PCR analysis (data not shown).

To confirm that the gene-targeting did not introduce additional sequence alterations in the *Parg* and *Timm23* genes of *Parg*$^{-/-}$ ES cell clones, we sequenced about 300 bp encompassing a 5'-junctional site of gene-targeting, in the *neo*^{r} and the *puro*^{r} allele, respectively, and found no sequence alteration in *Parg*$^{-/-}$ ES cell clones. We also sequenced approximately 500 bp of the *neo*^{r} allele, spanning a part of intron 1 and exon 1 of the *Timm 23*, *Timm23/Parg* promoter and *Parg* exon 1. The approximately 480 bp region of the *puro*^{r} allele, spanning the *Timm23 exon 1*, *Parg/Timm23* promoter, *Parg* exon 1 and the *puro*^{r} promoter was sequenced as well. Two serial gene-targeting events were suggested to produce the targeted alleles precisely and additional mutations were not found at the 5'-junctional site of gene-targeting in *Parg*$^{-/-}$ ES cell clones D79 and D122.

These results indicate that targeted disruption of *Parg* gene exon 1 eliminated the transcript, which encodes a full-length isoform of Parg, and also caused a marked reduction in the amount of other Parg transcripts encoding putative Parg isoforms.

In Vitro Growth of ES Cell Clones

Growth-rates of two *Parg*$^{-/-}$ ES cell clones, in the absence of a STO cell feeder layer were similar to those for parental J1 and *Parg*$^{+/-}$ ES cell clones. Doubling-time was calculated to be about 9 h in all cases and statistical differences in growth were not observed among the genotypes (Fig. **3A**). No proliferation impediment was observed in at least 50 successive passages in the absence of the feeder layer in each genotype.

Sensitivity of *Parg*$^{-/-}$ ES Cell Clones to DNA Damaging Agents of Various Types

Clonogenic survival assays revealed that *Parg*$^{-/-}$ ES cell clones show about 1.5-fold increased lethality with the monofunctional alkylating agent, DMS compared to their *Parg*$^{+/+}$ counterpart, as illustrated in Fig. (**3B**) ($p<0.05$). *Parp-1*$^{-/-}$ ES cell clone exhibited increased lethality only at

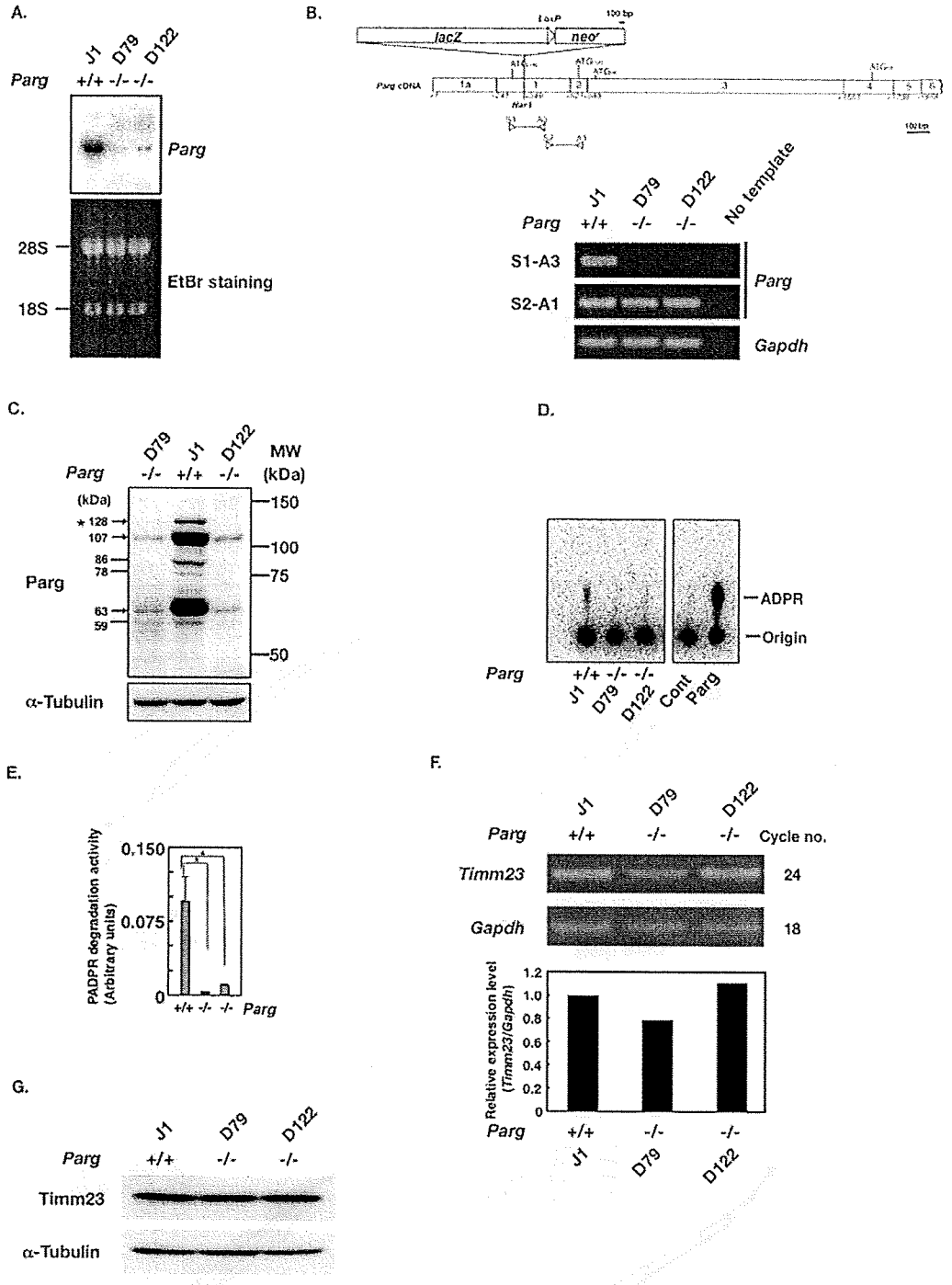

Fig. (2). **A.** Northern blot analysis. Thirty μg of total RNA isolated from ES cells was analyzed by Northern blot analysis using the *Parg* cDNA probe. **B.** Upper panel: Structure of the reported *Parg* cDNA in *Parg*$^{-/-}$ ES cell clones. The positions of primer set, S1 and A3, spanning the targeting site and another PCR set, S2 and A1, located downstream of the targeting site are shown. Lower panel: Total RNA isolated from ES cells was used to generate cDNAs and the PCR reaction was carried out using primer sets S1-S3 and S2-S1. **C.** Western blot analysis of Parg protein in ES cells. Total lysate of ES cells was subjected to western blot analysis using a monoclonal antibody against Parg and antibodies against α-tubulin. Arrows show major Parg isoforms and asterisks show minor Parg isoforms in *Parg*$^{+/+}$ ES cells. **D & E.** The measurement of poly(ADP-ribose) degradation activity in the crude extracts of ES cell clones by TLC. A representative result of the TLC (**D**). Cont, control. The quantification graph (**E**). Bar, mean ± SE. **F.** RT-PCR analysis of the *Timm23* gene. The length of the PCR product was 220 bp as expected. **G.** Western blot analysis of Timm23 in *Parg*$^{-/-}$ ES cells. Western blot analysis was carried out using a monoclonal antibody against Timm23 diluted at 1:2,500.